

# Fractal behavior of soil water storage at multiple depths

Wenjun Ji<sup>1</sup>, Mi Lin<sup>1</sup>, Asim Biswas<sup>1\*</sup>, Bing C. Si<sup>2</sup>, Henry W. Chau<sup>3</sup>, and Hamish P. Cresswell<sup>4</sup>

<sup>1</sup> Department of Natural Resource Sciences, McGill University, 2111 Lakeshore Road, Ste-Anne-de-Bellevue, Quebec, Canada, H9X3V9

<sup>2</sup> Department of Soil Science, University of Saskatchewan, Saskatchewan, Canada, S7N5A8

<sup>3</sup> Department of Soil and Physical Sciences, Lincoln University, PO Box 85084, Lincoln, Christchurch, New Zealand, 7647

<sup>4</sup> CSIRO Land and Water, Canberra, ACT, Australia, 2601

\* Correspondence to: A. Biswas ([asim.biswas@mcgill.ca](mailto:asim.biswas@mcgill.ca) Phone: +1 514 398 7620; Fax: +1 514 398 7990)

**Abstract** Spatio-temporal behavior of soil water is essential to understand the science of hydrodynamics. Data intensive measurement of surface soil water using remote sensing has established that the spatial variability of soil water can be described using the principle of self-similarity (scaling properties) or fractal theory. This information can be used in determining land management practices provided the surface scaling properties are kept at deep layer. Current study examined the scaling properties of sub-surface soil water and their relationship to surface soil water, thereby serving as supporting information for plant root and vadose zone models. Soil water storage (SWS) down to 1.4 m depth at seven equal intervals was measured along a transect of 576 m for 5 years in Saskatchewan. The surface SWS showed multifractal nature only during the wet period (from snowmelt until mid to late June) indicating the need for multiple scaling indices in transferring soil water variability information over multiple scales. However, with increasing depth, the SWS became monofractal in nature indicating the need for a single scaling index to upscale/downscale soil water variability information. The dynamic nature of the surface layer soil water in the wet period is highly variable compared to the deep layers. In contrast, all soil layers during the dry period (from late June to the end of the growing season in early November) were monofractal in nature, probably resulting from the high evapotranspirative demand of the growing vegetation that surpassed other effects. This strong similarity between the scaling properties at the surface layer and deep layers provides the possibility of inferring about the whole profile soil water dynamics using the scaling properties of the easy-to-measure surface SWS data.

**Keywords** Scale invariance, monofractal, multifractal, root zone, remote sensing

## 33 **1 Introduction**

34 Knowledge on the spatial distribution of soil water over a range of spatial scales and time has  
35 important hydrologic applications including assessment of land-atmosphere interactions  
36 (Sivapalan, 1992), performance of various engineered covers, monitoring soil water balance  
37 and validating various climatic and hydrological models (Rodriguez-Iturbe et al., 1995;Koster  
38 et al., 2004). However, high variability in soil is a major challenge in hydrology (Quinn, 2004)  
39 as the distribution of soil water in the landscape is controlled by various factors and processes  
40 operating at different intensities over a variety of extents (Entin et al., 2000). The individual  
41 and/or combined influence of these physical factors (e.g. topography, soil properties) and  
42 environmental processes (e.g. runoff, evapotranspiration, and snowmelt) gives rise to complex  
43 and nested effects, which in turn evolve a signature in the spatial organization (Western et al.,  
44 1999) or patterns in soil water as a function of spatial scale (Kachanoski and Dejong, 1988;Kim  
45 and Barros, 2002;Biswas and Si, 2011a). This complexity makes the management decision  
46 difficult at a scale other than the scale of measurement. Therefore, it is necessary to transfer  
47 variability information from one extent (e.g. pedon scale) to another (e.g. large catchment  
48 scale), which is called scaling.

49 The scaling of soil water is possible if the distribution of some statistical parameters (e.g.,  
50 variance) remain similar at all studied scopes. This feature, known as scale-invariance, means  
51 that the spatial feature in the distribution of soil water will not change if the length scales are  
52 multiplied by a common factor (Hu et al., 1997). Generally, the soil water will have a typical  
53 size or scale, a value around which individual measurements are centered. So the probability  
54 of measuring a particular value will vary inversely as a power of that value, which is known as  
55 the power law decay, a typical principle of scaling process. Now, as the spatial distribution of  
56 soil water follows the power law decay (Hu et al., 1997;Kim and Barros, 2002;Mascaro et al.,  
57 2010), the spatial variability can be investigated and characterized quantitatively over a large  
58 range of measurement extents using the fractal theory (Mandelbrot, 1982). When the spatial  
59 distribution of soil water is the response of some linear processes, the scaling can be done using  
60 a single coefficient over multiple scales and the distribution shows monofractal behavior.  
61 However, the spatial distribution of soil water is the nonlinear response of multiple factors and  
62 processes acting over a variety of scales and therefore needs multiple scaling indices  
63 (multifractals) for quantifying spatial variability (Hu et al., 1997;Kim and Barros,  
64 2002;Mascaro et al., 2010).

65 The multifractal behavior in the surface soil water as a result of temporal evolution of  
66 wetting and drying cycles have been reported from a sub-humid environment of Oklahoma by  
67 Kim and Barros (2002). Mascaro et al. (2010) reported the multifractal behavior of soil water,  
68 which was ascribed as a signature of the rainfall spatial variability. Though these measurements  
69 can provide a quick estimate of soil water over a large area, they are limited to very few  
70 centimeters of the soil profile. These studies reported the multifractal behavior of only the  
71 surface soil water indicating the superficial scaling properties. Surface soil layer is exposed to  
72 direct environmental forces and is the most dynamic in nature. The scaling properties of surface  
73 soil water can be used for land management practices provided the observed scaling properties  
74 remain the same characteristics for the deep layers such as vadose zone or the whole soil  
75 profile. Understanding overall hydrological dynamics in soil profile needs information on the  
76 scaling properties and the nature of the spatial variability of soil water over a range of scales at  
77 deep layers as well (Biswas et al., 2012b). The information on the similarity in the nature of  
78 the spatial variability of soil water between the surface layer and deep layers may also help  
79 inferring about the soil profile hydrological dynamics. Therefore, the objectives of this study  
80 were to examine over time the scaling properties of sub-surface layers and their relationship  
81 with surface layers at different initial soil water conditions. We have examined the scaling  
82 properties of soil water storage at each layer and their trend with increasing depth from the  
83 surface (cumulative depth) over a 5-year period from a hummocky landscape from central  
84 Canada using the multifractal analysis. The relationship between the scaling properties of the  
85 surface layer and the subsurface layers was also examined using the joint multifractal analysis.

## 86 **2 Materials and Methods**

### 87 **2.1 Study site and data collection**

88 A field experiment was carried out at St. Denis National Wildlife Area (52°12'N latitude,  
89 106°50'W longitude and ~549 m above sea level), which is located 40 km east of Saskatoon,  
90 Saskatchewan, Canada. The landscape of the study area is hummocky with a complex sequence  
91 of slopes (10 to 15%) extending from differently sized rounded depressions to irregular  
92 complex knolls and knobs, a characteristic landscape of the North American Prairie pothole  
93 region encompassing approximately 780,000 km<sup>2</sup> from north-central United States to south-  
94 central Canada (National Wetlands Working Group, 1997). Some of these potholes are  
95 seasonal in nature meaning to store water in the spring (wet period) and drying out during later  
96 summer and in fall season (dry period) (Fig. 1). Variables water distribution within the  
97 landscape and in different landform elements such as side slopes, knolls, and depressions

98 support vegetation differently. For example, the large amount of stored water in depressions  
99 provide a luxurious supply of water to growing plants compared to knolls (Fig. 1). A transect  
100 of 128 points (576 m long) extending in the north-south direction covering multiple knoll-  
101 depression cycles was established in 2004 at the study site to examine the soil water variation  
102 at field scale. The sample points were selected at 4.5 m regular intervals along the transect to  
103 catch the systematic variability of soil water. Soil water measurements were carried out at every  
104 20 cm depth down to 140cm along the transect over the period of 2007 to 2011, among which,  
105 the surface soil water (0 to 20 cm) was measured using vertically installed time domain  
106 reflectometry (TDR) probes and a metallic cable tester (Model 1502B, Tektronix, Beaverton,  
107 OR), while the rest deeper soil down to 140 cm depth was measured using a neutron probe  
108 (Model CPN 501 DR Depthprobe, CPN International Inc., Martinez, CA) (Biswas et al.,  
109 2012a). These measured data of soil water content from either the neutron probe or TDR were  
110 then multiplied with depth and added together to obtain the overall soil profile water storage  
111 so as to examine the fractal behavior of SWS at different depths over time A detailed  
112 description of the study site, development of the transect, measurement of soil water and the  
113 calibration of measurement instruments can be found in earlier publications from this project  
114 (e.g. Biswas et al. (2012a)).

## 115 **2.2 Data analysis**

116 Various methods including geostatistics, spectral analysis, and wavelet analysis have been used  
117 to examine the scale-dependent spatial patterns of SWS. These methods generally deal with  
118 how the second moment of SWS changes with scales or frequencies. When the statistical  
119 distribution of SWS is normal, the second moment plus the average provide a complete  
120 description of the spatial series. However, for other distributions (e.g. left skewed distribution),  
121 higher-order moments are necessary for a complete description of the spatial series. For  
122 example, let's define the  $q^{\text{th}}$  moment of a spatial series  $z$  as  $z^q$ . In this situation, for a positive  
123 value of  $q$ , the  $q^{\text{th}}$  moment magnify the effect of larger numbers and diminish the effect of  
124 smaller numbers in  $z$ . While, on the other hand, for a negative value of  $q$ , the  $q^{\text{th}}$  moment  
125 magnify the effect of small numbers and diminish the effect of large numbers in the spatial  
126 series  $z$ . In this way, using variable moments, we can look at the effect of the magnitude of the  
127 data in a series and better characterize its spatial variability.

### 128 **2.2.1 Statistical self-similarity or scale invariance**

129 Soil water is highly variable in space and time. If the variability in the spatial/temporal  
130 distribution remains statistically similar at all studied scales, the SWS is assumed to be self-  
131 similar (Evertsz and Mandelbrot, 1992). Self-similarity, also called scale invariance, is closely  
132 associated with the transfer of information from one scale to another. We used the multifractal  
133 analysis to explore self-similarity or inherent differences in scaling properties of SWS in this  
134 study.

### 135 **2.2.2 Multifractal analysis**

136 On the spatial domain of the studied field, multifractal analysis was used to characterize the  
137 scaling property of SWS by statistically measuring the mass distribution (Zelege and Si, 2004).  
138 The spatial domain or the data along the transect was successively divided into self-similar  
139 segments following the rule of the binomial multiplicative cascade (Evertsz and Mandelbrot,  
140 1992). This method required that the two segments divided from a unit interval to be of equal  
141 length. With regards to a unit mass  $M$  (a normalized probability distribution of a variable or  
142 measured in a generalized case) relating to the unit interval, the weight was also partitioned  
143 into  $[h \times M]$  and  $[(1-h) \times M]$ , where  $h$  was a random variable ( $0 \leq h \leq 1$ ) governed by a  
144 probability density function. Sequentially, the new subsets with their associated mass were  
145 equally divided into smaller parts. In this way, multifractal analysis was able to describe the  
146 scaling properties for the higher-order moments compared to semivariogram which can only  
147 measure the scaling properties of the second moment. In a special case, if the scaling properties  
148 do not change with  $q$ , the spatial series can be identified as monofractal, when one scaling  
149 coefficient is enough to characterize scaling property of SWS. Generally, the multifractal  
150 analysis is good at measuring the highly fluctuated mass (box size) within a scale interval. This  
151 also provides physical insights at all scales regardless of any ad hoc parameterization or  
152 homogeneity assumptions in the analysis (Schertzer and Lovejoy, 1987).

153 For SWS spatial series, the scale-invariant mass exponent, was termed as  $\tau(q)$  (Liu and  
154 Molz (1997):

$$155 \langle [\Delta z(x)]^q \rangle \propto x^{\tau(q)} \quad [1]$$

156 where  $z$  was the SWS spatial series,  $x$  was the lag distance and the symbol  $\propto$  indicated  
157 proportionality. The  $\tau(q)$  is widely used in multifractal analysis. If the plot of  $\tau(q)$  vs.  $q$  [or  $\tau(q)$   
158 curve] has a single slope (i.e. a linear line), then the series is a simple scaling (monofractal)  
159 type. If  $\tau(q)$  curve is nonlinear and convex (facing downward), then the series is a multiscaling  
160 (multifractal) type. In this study, we used the universal multifractal (UM) model of Schertzer

161 and Lovejoy (1987) to create a reference line that represented the perfect monofractal type of  
 162 scaling. Assuming the conservation in mean value of SWS, this model simulated a cascade  
 163 process with a scaling function in an empirical moment. It is thus used here to compare and  
 164 characterize the observed scaling properties with a reference to the monofractal behavior. The  
 165 goodness-of-fit between the  $\tau(q)$  curves and the UM model was tested using the chi-square test.  
 166 The sum of squared residuals (SSRs) between the  $\tau(q)$  curve and the UM model was also  
 167 calculated to test the deviation. The  $\tau(q)$  curves over the range of  $q$  values (in this study -15 to  
 168 15 at 0.5 intervals) were fitted with a linear regression line (referred to as a single fit). The  
 169 linear fitting of the  $\tau(q)$  curves with  $q < 0$  and  $q > 0$  (referred to as segmented fit) was also  
 170 completed. The difference between the mean of slopes and segmented fits (for positive and  
 171 negative  $q$  values) was checked using the Student's  $t$  test.

172 With similar manner to Eq. [1], the  $q^{\text{th}}$  order normalized probability measure of SWS,  
 173  $\mu(q, \varepsilon)$  (also known as the partition function), is proven to vary with the scale size, as below

$$174 \quad \mu_i(q, \varepsilon) = \frac{[p_i(\varepsilon)]^q}{\sum_i [p_i(\varepsilon)]^q} \propto (\varepsilon / L)^{\tau(q)} \quad [2]$$

175 where  $\varepsilon$  is scale size in the  $i^{\text{th}}$  segment and  $p_i(\varepsilon)$  is the probability of a measure.  $p_i(\varepsilon)$  and  
 176 measures the concentration of a variable of interest (e.g. SWS) by dividing the value of the  
 177 variable in the segment to the whole support length (e.g. to the whole transect of length  $L$  units)  
 178 (Meneveau et al., 1990; Evertsz and Mandelbrot, 1992). The mass exponent  $\tau(q)$  was related to  
 179 the probability of mass distribution of SWS.

180 Moreover, the fractal dimension of the subsets of segments in scale size  $\varepsilon$  was measured by  
 181 the multifractal spectrum  $f(q)$ . When a coarse Hölder exponent (local scaling indices) of  $\alpha$  was  
 182 in the limit as  $\varepsilon \rightarrow 0$ ,  $f(q)$  was calculated as below (Evertsz and Mandelbrot, 1992):

$$183 \quad f(q) = \lim_{\varepsilon \rightarrow 0} \left( \log \left( \frac{\varepsilon}{L} \right) \right)^{-1} \sum_i \mu_i(q, \varepsilon) \log \mu_i(q, \varepsilon) \quad [3]$$

184 and the local scaling indices,  $\alpha$ , were given by

$$185 \quad \alpha(q) = \lim_{\varepsilon \rightarrow 0} \left( \log \left( \frac{\varepsilon}{L} \right) \right)^{-1} \sum_i \mu_i(q, \varepsilon) \log p_i(\varepsilon) \quad [4]$$

186 Noting that  $f(\alpha)$  was determined through the Legendre transform of the  $\tau(q)$  curve:  
 187  $f(\alpha) = q\alpha(q) - \tau(q)$  (Chhabra and Jensen, 1989).

188 The multifractal spectrum is a powerful tool in portraying the similarity and/or differences  
 189 between the scaling properties of the measures (e.g. SWS). The width of the spectrum ( $\alpha_{\max}$  -  
 190  $\alpha_{\min}$ ) was used to examine the heterogeneity in the local scaling indices. The wider the  
 191 spectrum, the higher was the heterogeneity in the distribution of SWS and vice versa. Similarly,  
 192 the height of the spectrum corresponded to the dimension of the scaling indices. The small  $f(q)$   
 193 values indicated rare events (extreme values in the distribution), whereas the largest value was  
 194 the capacity dimension ( $D_0$ ) obtained at  $q = 0$ .

195 In addition to the multifractal spectrum, [ $f(q)$  vs.  $\alpha(q)$ ], for many practical applications, we  
 196 used models to incorporate a few selected indicators to describe the scaling property and  
 197 variability of a process. One of the widely used models for multifractal measure were the  
 198 generalized dimensions, which was calculated as below:

$$199 \quad D_q = \frac{1}{q-1} \lim_{\varepsilon \rightarrow 0} \frac{\log \sum_i p_i(\varepsilon)}{\log(\varepsilon)} \quad [5]$$

200 when  $q = 1$ ,  $D_1$  was referred to as the information dimension (also known as entropy dimension)  
 201 which provided information about the degree of heterogeneity in the measure distribution in  
 202 analogy to the entropy of an open system in thermodynamics (Voss, 1988). If the value of  $D_1$   
 203 is close to unity, it indicated the evenness of measures over the sets of cell size, while the value  
 204 approaching 0 indicated a subset of scale in which the irregularities were concentrated. The  $D_2$ ,  
 205 known as the correlation dimension, was associated with the correlation function and measured  
 206 the average distribution density of the SWS (Grassberger and Procaccia, 1983). For a  
 207 monofractal distribution, the  $D_1$  and  $D_2$  tend to be equal to the  $D_0$ . The same value of  $D_0$ ,  $D_1$   
 208 and  $D_2$  indicates that the distribution exhibits perfect self-similarity and is homogeneous in  
 209 nature. Contrarily, in multifractal type scaling, the  $D_1$  and  $D_2$  tend to be smaller than  $D_0$ ,  
 210 showing  $D_0 > D_1 > D_2$ . Accordingly, the  $D_1/D_0$  value can be used to describe the heterogeneity  
 211 in the distribution (Montero, 2005). When this value equals to 1, it indicated exact monoscaling  
 212 of the distribution.

### 213 **2.2.3 Joint multifractal analysis**

214 While the multifractal analysis characterized the distribution of a SWS spatial series along its  
 215 geometric support, the joint multifractal analysis was used to characterize the joint distribution  
 216 of two SWS spatial series along a common geometric support. As an extension of the  
 217 multifractal analysis, the length of the datasets was also divided into several segments of size

218  $\varepsilon$ . Two variables ( $P_i(\varepsilon)$  and  $R_i(\varepsilon)$  representing two spatial series of SWS) were used here to  
 219 measure the probability of the measure in the  $i^{\text{th}}$  segment, when  $P_i(\varepsilon) \propto (\varepsilon/L)^\alpha$  and  $R_i(\varepsilon) \propto (\varepsilon/L)^\beta$   
 220 . Among them,  $\alpha$  and  $\beta$  were the local singularity strength which respectively represented the  
 221 mean local exponents of  $P_i(\varepsilon)$  and  $R_i(\varepsilon)$  in the corresponding expressions above. The  
 222 partition function for the joint distribution of  $P_i(\varepsilon)$  and  $R_i(\varepsilon)$ , was calculated as below  
 223 (Chhabra and Jensen, 1989; Meneveau et al., 1990; Zeleke and Si, 2004):

$$224 \quad \mu_i(q, t, \varepsilon) = \frac{p_i(\varepsilon)^q \cdot r_i(\varepsilon)^t}{\sum_{j=1}^{N(\varepsilon)} [p_j(\varepsilon)^q \cdot r_j(\varepsilon)^t]} \quad [6]$$

225 where the normalized  $\mu$  is the partition function,  $q$  and  $t$  were the real numbers for weighting.  
 226 And the aforementioned local singularity strength (coarse Hölder exponents)  $\alpha$  and  $\beta$  were the  
 227 function to  $q$  and  $t$  as well:

$$228 \quad \alpha(q, t) = -[\ln(N(\varepsilon))]^{-1} \sum_{i=1}^{N(\varepsilon)} [\mu_i(q, t, \varepsilon) \cdot \ln(p_i(\varepsilon))] \quad [7]$$

$$229 \quad \beta(q, t) = -[\ln(N(\varepsilon))]^{-1} \sum_{i=1}^{N(\varepsilon)} [\mu_i(q, t, \varepsilon) \cdot \ln(r_i(\varepsilon))] \quad [8]$$

230 To indicate the dimension of the joint distribution, the multifractal spectra  $f(\alpha, \beta)$ , was given  
 231 by

$$232 \quad f(\alpha, \beta) = -[\ln(N(\varepsilon))]^{-1} \sum_{i=1}^{N(\varepsilon)} [\mu_i(q, t, \varepsilon) \cdot \ln(\mu_i(q, t, \varepsilon))] \quad [9]$$

233 In fact, the joint partition function in Eq. [6] can be simplified to Eq. [2] when  $q$  or  $t$  is equal  
 234 to 0. In this case, the joint multifractal spectrum was transformed to the multifractal spectrum  
 235 with a single measure. When both  $q$  and  $t$  were 0,  $f(\alpha, \beta)$  reached maximum and indicated  
 236 box dimension of the geometric support of the measures. Pair value of  $\alpha$  and  $\beta$  fluctuates with  
 237 the change of variable  $q$  and  $t$ . Therefore, it is possible to examine the distribution of high or  
 238 low values (different intensity levels) of one variable with respect to another by varying the  
 239 values of  $q$  or  $t$ . As the joint multifractal spectra  $f(\alpha, \beta)$  represents the frequency of the  
 240 occurrence of certain values of  $\alpha$  and  $\beta$ , high values of  $f(\alpha, \beta)$  represents strong association  
 241 between the values of  $\alpha$  and  $\beta$ . The Pearson correlation coefficient was used to quantitatively



242 describe their relations across similar moment orders. In addition, correlation coefficients  
243 between the surface layer and subsurface layers were used as well to examine the similarity in  
244 the scaling properties. Additionally, a contour was used to represent the joint distribution of a  
245 pair of variables by permuting similar values (highs vs highs or lows vs lows) of  $q$  and  $t$ . The  
246 bottom left part of the contour graph presents the joint distribution of high data values of both  
247 variables while top right part represents the low data values of both variables. Therefore, a  
248 diagonal contour with low stretch indicate strong association between the variables in  
249 consideration (Biswas and Si, 2012b).

### 250 **3 Results**

#### 251 **3.1 Spatial pattern of soil water storage at different depths**

252 Average SWS for the surface 0-20 cm layer over five year period was 5.51 cm. A slight  
253 decrease in SWS was observed at the immediate deep layer (20-40 cm) and a gradual increase  
254 thereafter. Five-year average SWS was 5.45 cm, 5.48 cm, 5.56 cm, 5.61 cm, 5.69 cm and 5.77  
255 cm for the 20-40 cm, 40-60 cm, 60-80 cm, 80-100 cm, 100-120 cm and 120-140 cm layers,  
256 respectively. Average SWS for a single measurement varied from 3.40 cm to 7.16 cm. The  
257 highest average SWS for the surface layer was observed on 29 June 2011. The study area  
258 received large amount of spring snowmelt (2010 received 642 mm, double the annual average  
259 precipitation) and rainfall during 2011 leading to the high SWS in the surface layer (Weather  
260 Canada historical report). The lowest average SWS for surface was observed on 23 August  
261 2008, which was one of the driest summers within the five-year study period. The highest  
262 average SWS (on 29 June 2011) at the surface layer gradually decreased to 6.55 cm and the  
263 lowest average SWS (on 23 August 2008) at the surface layer gradually increased to 5.28 cm  
264 at the 120-140 cm layer (Table 1). These top and bottom boundaries formed a wider range  
265 (3.76 cm) of the average SWS at the surface layer compared to that at the deepest layer (1.27  
266 cm). A big range (2.00 cm) in the standard deviation (maximum=2.43 cm and minimum=0.43  
267 cm) of the measurement at the surface layer (0-20 cm) was also observed compared to that at  
268 the deepest layer (120-140 cm; maximum=1.28 and minimum=0.76). This indicated large  
269 variations in SWS at the surface layer and gradually decreased at deeper layers. The  
270 coefficients of variation (CVs) at the surface layer (0-20 cm) varied from 10% to 43% and the  
271 deepest layer (120-140 cm) varied from 13% to 23% (Supplementary Table S.1).

272 The maximum SWS at the surface layer also varied widely (maximum=13.96 cm and  
273 minimum=4.64 cm) compared to the deepest layer (maximum=9.81 cm and minimum=6.71

274 cm) (Table 1). There was a gradual decrease in the maximum value and increase in the  
275 minimum value from the surface to the deepest layer. A similar trend was also observed for the  
276 minimum SWS at different layers. The maximum SWS at different layers was much localized.  
277 For example, there was high SWS at different layers at the locations of 100 to 140 m and 225  
278 to 250 m from the origin of the transect. These locations had very high SWS compared to the  
279 field-average because they were situated in the depressions while low SWS was observed on  
280 the knolls.

281 The variations in SWS with time were evaluated within a year. There was little change in  
282 the average SWS over measurements within the years from 2007-2011 except 2008 (Table 1).  
283 For example, average SWS was 6.47 cm, 6.03 cm, 6.54 cm, and 6.33 cm on 6 April 2010, 19  
284 May 2010, 14 June 2010 and 28 September 2010, respectively. However, the average SWS in  
285 2008 drops from 6.28 cm on 2 May 2008 to 3.51 cm on 17 September 2008 in the surface 0-  
286 20 cm layer. This falling trend was observed at all soil layers. When compared between years,  
287 the trend over time and with depth was very similar in 2007 and 2009 while slightly different  
288 between 2010 and 2011 (Table 1). A decreasing trend of the variability was also observed with  
289 time. For example, the CV of the surface layer was around 28% on 2 May 2008, which  
290 gradually decreased to around 13% on 17 September 2008 (Supplementary Table S.1).

291 The average water storage for soil layers with increasing depth was also calculated by  
292 adding the individual layers together. The time-averaged values of SWS were 10.96 cm, 16.44  
293 cm, 22.00 cm, 27.61 cm, 33.30 cm and 39.07 cm for the 0-40 cm, 0-60 cm, 0-80 cm, 0-100 cm,  
294 0-120 cm and 0-140 cm, respectively (Supplementary Table S.2). The CV of the 0-20 cm layer  
295 was the highest during the wet period and gradually declined to the smallest during the dry  
296 period (Supplementary Table S.3). The variability also gradually increased with depth.

### 297 **3.2 Statistical scale invariance**

298 The power law relationships and the statistical scale invariance were evaluated using a log-log  
299 plot of the aggregated variance of SWS spatial series at different depths of soil layers and the  
300 level of disaggregation (or scales) at different  $q$  values or statistical moments. The linear  
301 relationship of the logarithm of the variance with scale indicated the presence of statistical scale  
302 invariance (Fig. 2). The scale invariance was observed for all measurements and at all depths  
303 though only all depths of selected three dates were presented as example. The coefficient of  
304 determination ( $r^2$ ) for a linear fit ( $n=7$ ) was between 0.99 and 1.00 (significant at  $P=0.001$ ) for

305 any measurement days and depths. The scale invariance was also observed for SWS trend with  
306 increasing depths.

### 307 **3.3 Multifractal analysis**

308 The  $\tau(q)$  curves for the surface layer displayed deviation from the UM model during the wet  
309 period (Fig. 3). A high SSR value was observed between the  $\tau(q)$  curves and the UM model.  
310 Nonlinearity in the  $\tau(q)$  curve was observed and the slopes of the segmented fit of the  $\tau(q)$   
311 curves were significantly different from each other. For example, the SSR values between the  
312  $\tau(q)$  curve and the UM model were 27.74 and 50.49 for the surface layer (0-20 cm) on 2 May  
313 2008 and 31 May 2008, respectively. The slopes of the  $\tau(q)$  curve for (single fit) were 0.97 and  
314 0.96, respectively for the surface layer of 2 May 2008 and 31 May 2008 (Fig. 3). The slopes of  
315 the segmented fit for these measurements were 1.04 ( $q < 0$ ) and 0.87 ( $q > 0$ ) and, 1.06 ( $q < 0$ ) and  
316 0.82 ( $q > 0$ ), respectively (Fig. 3; Supplementary Table S.4).

317 With the maximum deviation at the surface layer, the  $\tau(q)$  curves gradually became very  
318 similar to the UM model with depth. The SSR value decreased considerably in deep layers.  
319 The slopes of the  $\tau(q)$  curve (single fit) became almost unity with no significant difference with  
320 the UM model. There was no significant difference between the slopes of the segmented fit.  
321 For example, the SSR value was 6.17, 4.98, 8.80, 8.50, 8.86, and 6.16 respectively for the 20-  
322 40, 40-60, 60-80, 80-100, 100-120, and 120-140 cm layer of 2 May 2008 (Supplementary Table  
323 S.4). The slopes (single fit) for these layers were 0.99, 1.00, 1.01, 1.01, 1.00, and 0.99,  
324 respectively (Fig. 3). The slopes of the segmented fit were also very close to unity with no  
325 significant difference between them.

326 The SSR values gradually decreased and the slopes became almost unity with increasing  
327 depth of soil layers (Fig. 4). For example, the SSR values were 14.11, 9.31, 7.71, 6.86, 6.71  
328 and 6.30 and the slopes (single fit) were 0.98, 0.99, 0.99, 1.00, 1.00, and 1.00, respectively for  
329 0-40, 0-60, 0-80, 0-100, 0-120 and 0-140 cm layer (Supplementary Table S.5). The slopes of  
330 the segmented fit for the  $\tau(q)$  curve became almost the same as soil layers went deeper (Fig. 4).  
331 The linearity of the  $\tau(q)$  curves was gradually strengthened and the SSR value gradually fell  
332 with the depth increase of soil layers at any time. A significant difference was observed  
333 between the slopes of the  $\tau(q)$  curves in segmented fitting at the surface layer of the first three  
334 measurements in 2007 (Supplementary Fig. S.1), two measurements in 2008 (Fig. 4), three  
335 measurements in 2009 and all measurements in 2010 and 2011 (Supplementary Fig. S.2).

336 A decreasing trend in the SSR value was also observed over time within a year. During the  
337 dry period, the slopes (single fit and segmented fit) became almost unity with no significant  
338 difference (Supplementary Table S.6). For example, the SSR value was 14.12, 8.25, 1.30, 1.46,  
339 and 0.52 and the slope was 0.99, 0.99, 1.00, 1.00, and 1.00, respectively for the surface layer  
340 (0-20 cm) of 21 June 2008, 16 July 2008, 23 August 2008, 17 September 2008 and 22 October  
341 2008 (Fig. 3). Similarly, a small SSR value and consistent slope were also observed at the  
342 deepest layer (120-140 cm). The SSR values of the 120-140 cm were 2.47, 2.47, 3.31, 3.44 and  
343 4.57, respectively for the measurements on 21 June 2008, 16 July 2008, 23 August 2008, 17  
344 September 2008 and 22 October 2008 (Supplementary Table S.6). The slope (single fit) for all  
345 these measurements was equal to 1.01 (Fig. 3). There was very little difference in the slopes of  
346 the segmented fits.

347 A significant difference in the slopes of the segmented fit was observed for the surface  
348 layer (0-20 cm) of three measurements in 2007 (17 July, 7 August, and 1 September;  
349 Supplementary Fig. S.1), and three measurements in 2009 (21 April, 7 May, and 27 May)  
350 (Supplementary Table S.4; Supplementary Fig. S.2). The difference became non-significant  
351 with depth and during other measurement times. The trend in deep layers over time was very  
352 similar to that of 2008. However, the trend in the SSR values and the slopes with time was  
353 different in 2010 and 2011 (Supplementary Table S6). There was very little difference in the  
354 SSR values at different times of the year. For example, the SSR value for the surface layer (0-  
355 20 cm) was 20.79, 27.18, 24.63 and 26.66 and the slope (single fit) was 0.97, 0.97, 0.97, and  
356 0.97, respectively for the measurements on 6 April 2010, 19 May 2010, 14 June 2010, and 28  
357 September 2010 (Fig. 3). The slope of the segmented fit of the surface layer (0-20 cm) was  
358 statistically significant for all measurements in 2010 and 2011. However, the trend with depth  
359 was similar to other years (Supplementary Table S.7).

360 The height of the multifractal spectrum at different depths of measurement was very similar  
361 over time. The width of the spectrum ( $\alpha_{\max}-\alpha_{\min}$ ) varied with depth and time (Fig. 5). Generally,  
362 a comparative large value of  $\alpha_{\max}-\alpha_{\min}$  was observed at the surface layer during the wet period  
363 and the value gradually became smaller with depths. For example, the value of  $\alpha_{\max}-\alpha_{\min}$  for  
364 the surface soil layer (0-20 cm) was 0.23 and 0.31, respectively for the measurements of 2 May  
365 2008 and 31 May 2008 (Fig. 5). Meanwhile, the value of  $\alpha_{\max}-\alpha_{\min}$  for the soil layers of 20-140  
366 cm with 20 cm increment was 0.15, 0.14, 0.19, 0.20, 0.20, and 0.18 for 2 May 2008 and 0.25,  
367 0.19, 0.11, 0.14, 0.12, and 0.11 for 31 May 2008, respectively (Fig. 6). In the later part of the  
368 year, the width of the spectrum gradually decreased (Supplementary Table S.8). For example,

369 the  $\alpha_{\max}-\alpha_{\min}$  values were 0.19, 0.16, 0.07, 0.08, and 0.05, respectively for the surface layer on  
370 21 June 2008, 16 July 2008, 23 August 2008, 17 September 2008 and 22 October 2008. Similar  
371 trend in values of  $\alpha_{\max}-\alpha_{\min}$  was also observed at deep layers (Fig. 6).

372 The trend of the  $\alpha_{\max}-\alpha_{\min}$  values in 2007 and 2009 was very similar to that of 2008  
373 (Supplementary Table S.8). A higher value of  $\alpha_{\max}-\alpha_{\min}$  was observed in the first three  
374 measurements of 2007 (Supplementary Fig. S.5) and three measurements of 2009  
375 (Supplementary Fig. S.6). However, the values in the surface layer (0-20 cm) of measurements  
376 in 2010 and 2011 were always higher compared to the deep layers (Fig. 6). There was no  
377 decreasing trend in values for the surface layer over time. For example, the  $\alpha_{\max}-\alpha_{\min}$  value was  
378 0.21, 0.24, 0.21, and 0.22, respectively for the measurements on 6 April 2010, 19 May 2010,  
379 14 June 2010, and 28 September 2010 (Fig. 6). However, the trend in the  $\alpha_{\max}-\alpha_{\min}$  value of  
380 deep layers was similar to that of other years. A similar trend was observed for cumulative  
381 SWS with increasing depth over the years (Fig. 7). Generally, the value of  $\alpha_{\max}-\alpha_{\min}$  was also  
382 small with the highest in the 0-20 soil layers and gradually decreased with depth (Fig. 7;  
383 Supplementary Table S.9).

384 A very similar height of the  $f(q)$  curve for all depths and all periods indicated a consistent  
385 frequency distribution of the scaling indices (Fig. 6 and 7). Additionally, the position and the  
386 symmetry of the curve revealed the distribution of scaling exponents. A symmetric  $f(q)$  curve  
387 indicated uniform distribution of the scaling exponents. The left side of the spectrum  
388 corresponded to the large SWS that were amplified by the positive values of  $q$  while the right  
389 side indicated smaller SWS that were amplified by negative  $q$  values. Symmetry leaning  
390 towards the left side during the early spring and in the surface layers in 2008 clearly showed  
391 the wider distribution of scaling indices and multifractal nature of the SWS (Fig. 6). While the  
392 shifting of the symmetry towards right side clearly indicated less variable scaling indices and  
393 thus reduction of multifractal behavior. During the wet year of 2010 and 2011, the symmetry  
394 towards left side indicated the variability in the scaling indices. This also persisted with depth.  
395 A similar trend was observed for different years at all layers of cumulative depths (Fig. 7).

396 Generally, the  $D_1$  and  $D_2$  values for different depths of different measurements were very  
397 close to 1 (only varied at 3 decimal points; Fig. 8 and Supplementary Table S.10). In general,  
398 the  $D_1$  value of the surface layers gradually increased with depth. Similarly, at any depth, the  
399  $D_1$  values gradually increased from spring to fall season through summer (Fig. 8). Highest  
400 variation in  $D$  values with  $q$  was observed in the surface layer and in the spring season and  
401 gradually decreased with depth and later part of the growing season. For example, the first

402 three measurements in 2007 and 2009 presented high  $D$  values at high  $q$  values (Supplementary  
403 Figs. S.9 and S.10). This high  $D$  value gradually decreased in the dry period of the year. For  
404 example, the  $D$  value with positive  $q$  was high in the surface layer of 2 May 2008 and 31 May  
405 2008 (Fig. 9), whereas it gradually decreased at the later part of the year (e.g. 17 September  
406 2008). The trend with time and depth in 2007 and 2009 was very similar to that of 2008  
407 (Supplementary Tables S.10 and S.11). A consistent high  $D$  value was observed in the surface  
408 layer for all 2010 and 2011 measurements (Fig. 9). The trend in  $D$  values with depth in 2010  
409 and 2011 was also similar to other years. A high value of  $D_1$  and  $D_2$  were also observed at all  
410 layers of cumulative depths for all measurements (Fig. 10; Supplementary Table S.11).

### 411 **3.4 Joint multifractal analysis**

412 There were strong correlations between the scaling property of the joint distribution of the  
413 surface soil layer and the deep soil layers. The narrow width and the diagonally oriented  
414 contours between SWS measured on 22 October 2008 at 0-20 cm and 20-40 cm layers clearly  
415 demonstrates strong association between those two layers (Fig. 11). The correlation between  
416 the surface 0-20 cm and the deep layers on 2 May 2008 (wet period) was larger than 0.9  
417 (significant at  $P=0.001$ ; Table 2). The highest correlation was observed between the layers  
418 closest to each other. The correlations gradually increased over time and showed high  
419 consistency between different layers on 17 September 2008 (Table 2). A very similar trend was  
420 observed in other years.

## 421 **4 Discussion**

422 The amount of water stored in the soil is the result of the dominant underlying hydrological  
423 processes. Located in semi-arid climate, the study area receives about 30% of the long term  
424 annual average precipitation as snowfall during winter months (Pomeroy et al., 2007).  
425 Generally, the depressions receive snow from surrounding uplands or knolls as redistributed  
426 by strong prairie wind (Pomeroy and Gray, 1995; Fang and Pomeroy, 2009). The snow melts  
427 within a short period of time during the early spring and contributes a large amount of water.  
428 The frozen ground restricts infiltration and redistributes excess water within the landscape with  
429 greater accumulation in depressions (Fig. 1) (Gray et al., 1985). Apart from the snowmelt, the  
430 spring rainfall also contributes to the water inflow in the landscape (Fig. 1). This created a  
431 spatial pattern of SWS that was almost a mirror image of the spatial distribution of relative  
432 elevation (Biswas and Si, 2011a, b; Biswas et al., 2012a).

433 In the spring, the sources of water loss were the deep drainage and the evaporation. As the  
434 loss of water through deep drainage in the study area was as low as 2 to 40 mm per year,  
435 occurring mainly through the fractures and preferential flow paths (Hayashi et al., 1998;van  
436 der Kamp et al., 2003), the major loss occurred mainly through evaporation from the surface  
437 of the bare ground and standing water in depressions. These processes lose a very small amount  
438 of water compared to the input of water in spring and early summer leaving the soil wet.  
439 Moreover, the surface soil with high organic matter content and low bulk density stored a larger  
440 amount of water than the deep layers where the organic matter gradually decreased and the  
441 bulk density increased. Reflecting the long-term history of vegetation growth in the landscape,  
442 the variability of organic matter content (CV=41%) may be one of the main factor of the high  
443 variability in surface layer SWS (Biswas and Si, 2011c).

444 As the vegetation developed in summer, strong evapotranspiration resulted in the lowest  
445 average SWS. High amount of water in the depressions allowed grasses to grow faster and  
446 transpire more water compared to the knolls (Fig. 1). For example, the aquatic vegetation  
447 growth within the depressions was as high as 2 m, while the grasses on the knolls grew to a  
448 maximum up to a meter tall. The uneven growth of vegetation and the high evapotranspirative  
449 demand in summer narrowed the range of SWS. In the soil where water is more available,  
450 evapotranspiration will be stronger while the less evapotranspirative demand will be shown in  
451 the relatively dry soil. As a result, the excessive water in the relatively wet soil will be offset  
452 by evapotranspiration, reducing the disparities between maximum and minimum values. This  
453 variable water uptake was visible in the growth of vegetation in the later part of the growing  
454 season as well (Fig. 1). The reduction in the range of SWS was the largest in the surface layer  
455 and gradually decreased at deeper layers. This is because the surface layer was exposed to  
456 various environmental forces. For example, plants can take up more than 70% of the water  
457 they need from the top 50% of the root zone (Feddes et al., 1978). This dynamic behavior of  
458 the surface layer exhausted readily available water and finally reduced the range in water  
459 storage. This decrease in range also happened in the later part of the growing season.

460 The multifractal and joint multifractal analyses explained the scaling behavior of SWS at  
461 different depths over time. The linearity in the log-log plot between the aggregated variance in  
462 SWS and the scale at all soil layers over time indicated that SWS behaved under scaling laws  
463 (Fig. 2). The near unity slope of the  $\tau(q)$  curves and the insignificant difference from the UM  
464 model indicated a monofractal type scaling at all layers except the surface layer during the wet  
465 period (until mid to late June) where a multifractal behavior led to a slight convex downward

466 curve (Fig. 3). This was also supported by a significant difference between the slope of single  
467 and segmented fit in the surface layer during the wet period.

468 Generally during the wet period, excess water fills and drains macropores quickly and  
469 creates variations in SWS. Variations in the evaporation due to uneven solar incidence over  
470 micro-topography also triggered SWS variability in the surface layer. Additionally, the snow  
471 melt and the release of water controlled by local (e.g. soil texture) and non-local (e.g.  
472 topography) factors also affected the spatial distribution of SWS, making it more heterogeneous  
473 in the wet period (Grayson et al., 1997; Biswas and Si, 2012). Contrarily, as depth increased,  
474 less impact of environmental factors tended to create less variability in SWS and exhibited a  
475 monofractal behavior which was consistent with the uniform slope shown in Figure 3. During  
476 the dry period or later part of the growing season, the SWS storage variability at all depths was  
477 small and exhibited monofractal behavior (Fig. 3). Accordingly, the deeper layers in the wet  
478 period and all layers in the dry period can be accurately represented by only one scaling  
479 exponent while the surface layer in the wet period may require a hierarchy of exponents. A  
480 similar trend was observed in SWS of cumulative depth layers (Fig. 4). Resulting from  
481 increasingly buffering capacity of the deeper soil layers, the variability of cumulative SWS  
482 overlaid the multifractal nature of the surface layer, and finally exhibited monofractal behavior  
483 in general.

484 The scaling patterns of SWS at different depths and different periods were further examined  
485 using multifractal spectrum [ $f(q)$  vs.  $\alpha(q)$ ] (Fig. 6 & Fig. 7). The degree of convexity was used  
486 to characterize the heterogeneity of scaling exponents or the degree of multifractality. Large  
487 value of  $\alpha_{\max}-\alpha_{\min}$  indicated stronger heterogeneity in the local scaling indices of SWS or  
488 cumulative SWS and vice versa. The largest value for the surface layer(s) in the wet period  
489 indicated the most multifractal behavior of SWS. However, the value decreased with depth and  
490 gradually converged in deep layers (Fig. 6). This decline manifested a conformity in the scaling  
491 behavior of SWS at deeper layers. Over time, the  $\alpha_{\max}-\alpha_{\min}$  value of the surface soil layer  
492 decreased and became very similar to that of deep layers. This indicated a reduction in the  
493 degree of multifractality for surface soil layers from the wet period to the dry period. A  
494 consistent  $\alpha_{\max}-\alpha_{\min}$  value for all depths during the dry period suggested the homogeneity and  
495 least multifractal nature of SWS. A similar behavior was observed in the cumulative SWS (Fig.  
496 7).

497 To sum up, both the unity slope of the  $\tau(q)$  curves (Fig. 3 and Fig. 4) and the degree of  
498 convexity of the  $f(q)$  spectrum (Fig. 6 & Fig. 7) jointly demonstrated that dynamic behavior of



499 surface soil layers in the wet period made SWS highly variable and exhibited multifractal  
500 nature, while less environmental forces and increased buffering capacity of deep layers led to  
501 monofractal nature. As a result, multiple scaling exponents were required to characterize the  
502 variability of SWS in the surface layer during the wet period, while less number of exponents  
503 was necessary for deeper layers during wet period or all layers during dry period.

504 The height of the spectrum,  $f(q)$  revealed the dimension or frequency distribution of the scaling  
505 indices (Caniego et al., 2003). A low height of  $f(q)$  curve indicated rare events or extreme  
506 values in the distribution, while a high value represented uniform distribution in all segments.  
507 A very similar height of the  $f(q)$  curve for all depths and all periods indicated a consistent  
508 frequency distribution of the scaling indices.

509 The two upper soil layers during the wet period tended to exhibit longer tail of the curve  
510 on the left, showing more heterogeneity in the distribution of large values. However, when  
511 stepping into the dry period, the spectrum tended to display a longer tail on the right compared  
512 to the left side, suggesting more heterogeneity in the distribution of smaller values. A few  
513 locations with standing water leads to the spatial differences during the wet period while a few  
514 points with very small SWS due to high evapotranspiration by growing vegetation during the  
515 dry period results in the heterogenic distribution in smaller values.

516 The generalized dimension,  $D_q$  was subsequently used to characterize the scaling property  
517 and variability in SWS (Fig. 9 and Fig. 10). The largest value of  $f(q)$ , referred to as the capacity  
518 dimension ( $D_0$ ) obtained at  $q = 0$ , was close to unity for all layers at different times (Fig. 9).  
519 The information dimension ( $D_1$ ) obtained at  $q = 1$  was different from correlation dimension  
520 ( $D_2$ ), which is denoted as the average distribution density of the measurement for the surface  
521 layers in the wet period (Grassberger and Procaccia, 1983). In this case, the different values of  
522  $D_0$ ,  $D_1$  and  $D_2$  indicated multifractal nature of the distribution of SWS. Similarly, a non-unity  
523 value of  $D_1/D_0$  (Montero, 2005) also indicated the multifractal nature of SWS at the surface  
524 layer(s) during the wet period. However, over the growing season, the  $D_1$  and  $D_2$  value  
525 approached to  $D_0$  and indicated a monofractal type behavior. Similar values of  $D_0$ ,  $D_1$  and  $D_2$   
526 during the dry period also indicated homogeneous distributions.

527 Joint multifractal distribution between the surface to various subsurface layers indicated  
528 the similarity in the scaling patterns (Table 2). Basically, the hydrological processes of  
529 shallower layers were similar to those of the top layer, while deeper layers showed more  
530 disparities from the surface. The nearest subsurface (20-40 cm) layer showed generally the

531 highest similarity with the surface (0-20 cm) layer. However, in the wet period, the subsurface  
532 layers displayed the smallest similarity to the surface layer, suggesting a higher dynamic nature  
533 of hydrological processes. In the dry period, a stronger effect of vegetation overwhelmed the  
534 effect of small variations of water distribution, thus creating a more uniform distribution of  
535 SWS at all soil layers and showed stronger similarity to the surface layers (Table 2).

536 Overall, our result revealed a multifractal behavior of surface soil layers during the wet  
537 period due to its dynamic nature of hydrological processes. This behavior gradually changed  
538 with depth and time (Fig. 12). In the deeper layers during the wet period, the behavior became  
539 less multifractal or nearly monofractal. Similarly, in the dry period, the vegetation development  
540 and its high evapotranspirative demand in the semi-arid climate of the study area increasingly  
541 buffered the variation of SWS, as a result, all the soil layers with less effect from environment  
542 factors showed uniform distribution or monofractal behavior (Fig. 12).

## 543 **5 Summary and Conclusions**

544 The transformation of information on soil water variability from one scale to another requires  
545 knowledge on the scaling behavior and the quantification of scaling indices. Surface soil water  
546 can be easily measured (e.g. remote sensing) and presents multi-scaling behavior (requiring  
547 multiple scaling indices). However, land-management practices require the understanding of  
548 the hydrological dynamics in the root zone and/or the whole soil profile.

549 In this manuscript, the scaling properties of soil water storage at different soil layers  
550 measured over a five-year period were examined using multifractal and joint multifractal  
551 analysis. The scaling properties of soil water storage mainly suggested a monofractal scaling  
552 behavior. However, the surface layer in the wet period or with high soil water storage tended  
553 to be multifractal, which gradually became monofractal with depths. With the decrease in soil  
554 water storage, the scaling behavior became monofractal during the growing season. In the year  
555 with high annual precipitation, the soil stored more water in the surface layer throughout the  
556 growing period and displayed nearly multifractal scaling behavior. This multifractal nature  
557 indicated that the transformation of information from one scale to another at the surface layer  
558 during the wet period requires multiple scaling indices. On the contrary, the transformation  
559 requires a single scaling index during the dry period for the whole soil profile. The scaling  
560 properties of the surface layer were highly correlated with that of the deep layers, which  
561 indicated a highly similar scaling behavior in the soil profile. The study was conducted in an  
562 undulating landscape from a semi-arid climate and the results were very consistent over the

563 years. Therefore, the observation completed at the field scale in this type of landscape and  
564 climate may be generalized in similar landscapes and climatic situations, otherwise may need  
565 to be examined thoroughly. The method used here can be transferred to examine the scaling  
566 properties in other experimental situations.

## 567 **6 Acknowledgements**

568 The project was funded by the Natural Science and Engineering Research Council of Canada.  
569 The help from the graduate student and the summer students of the Department of Soil Science  
570 at the University of Saskatchewan in collecting field data is highly appreciated.

## 571 **7 References**

- 572 Biswas, A., and Si, B. C.: Scales and locations of time stability of soil water storage in a  
573 hummocky landscape, *J. Hydrol.*, 408, 100-112, 10.1016/j.jhydrol.2011.07.027, 2011a.
- 574 Biswas, A., and Si, B. C.: Revealing the Controls of Soil Water Storage at Different Scales in  
575 a Hummocky Landscape, *Soil Sci. Soc. Am. J.*, 75, 1295-1306, 10.2136/sssaj2010.0131,  
576 2011b.
- 577 Biswas, A., and Si, B. C.: Identifying scale specific controls of soil water storage in a  
578 hummocky landscape using wavelet coherency, *Geoderma*, 165, 50-59,  
579 10.1016/j.geoderma.2011.07.002, 2011c.
- 580 Biswas, A., Chau, H. W., Bedard-Haughn, A. K., and Si, B. C.: Factors controlling soil water  
581 storage in the hummocky landscape of the Prairie Pothole Region of North America, *Can.*  
582 *J. Soil Sci.*, 92, 649-663, 10.4141/cjss2011-045, 2012a.
- 583 Biswas, A., and Si, B. C.: Identifying effects of local and nonlocal factors of soil water storage  
584 using cyclical correlation analysis, *Hydrol. Proc.*, 26, 3669-3677, 10.1002/hyp.8459, 2012.
- 585 Biswas, A., Zeleke, T. B., and Si, B. C.: Multifractal detrended fluctuation analysis in  
586 examining scaling properties of the spatial patterns of soil water storage, *Nonlin. Proc.*  
587 *Geophys.*, 19, 227-238, 10.5194/npg-19-227-2012, 2012b.
- 588 Biswas, A., and Si, B. C.: Application of multifractal and joint multifractal analysis in  
589 examining soil spatial variation: A review, *In* Quadfeul, S. (ed.), *Fractal analysis and chaos*  
590 *in Geosciences*. p. 109-138, 2012 c.
- 591 Caniego, F.J., Martín, M.A. and San José, F.: Rényi dimensions of soil pore size distribution.  
592 *Geoderma*, 112, 205– 216, 2003.
- 593 Chhabra, A., and Jensen, R. V.: Direct determination of the  $f(\alpha)$  singularity spectrum, *Physical*  
594 *Review Letters*, 62, 1327-1330, 1989.
- 595 Entin, J. K., Robock, A., Vinnikov, K. Y., Hollinger, S. E., Liu, S. X., and Namkhai, A.:  
596 Temporal and spatial scales of observed soil moisture variations in the extratropics, *J.*  
597 *Geophys. Res.-Atm.*, 105, 11865-11877, 10.1029/2000jd900051, 2000.
- 598 Evertsz, C. J. G., and Mandelbrot, B. B.: Self-similarity of harmonic measure on DLA, *Physica*  
599 *A: Statistical Mechanics and its Applications*, 185, 77-86, [http://dx.doi.org/10.1016/0378-4371\(92\)90440-2](http://dx.doi.org/10.1016/0378-4371(92)90440-2), 1992.
- 601 Fang, X., and Pomeroy, J. W.: Modelling blowing snow redistribution to prairie wetlands,  
602 *Hydrol. Proc.*, 23, 2557-2569, 10.1002/hyp.7348, 2009.
- 603 Feddes, R. A., Kowalik, P. J., and Zaradny, H.: *Simulation of field water use and crop yield.*,  
604 John Wiley & Sons Inc., New York, 1978.
- 605 Grassberger, P., and Procaccia, I.: Characterization of Strange Attractors, *Physical Review*  
606 *Letters*, 50, 346-349, 1983.

607 Gray, D. M., Landine, P. G., and Granger, R. J.: SIMULATING INFILTRATION INTO  
608 FROZEN PRAIRIE SOILS IN STREAMFLOW MODELS, *Can. J. Earth Sci.*, 22, 464-  
609 472, 1985.

610 Grayson, R. B., Western, A. W., Chiew, F. H. S., and Bloschl, G.: Preferred states in spatial  
611 soil moisture patterns: Local and nonlocal controls, *Water Resour. Res.*, 33, 2897-2908,  
612 1997.

613 Hayashi, M., van der Kamp, G., and Rudolph, D. L.: Water and solute transfer between a prairie  
614 wetland and adjacent uplands, 2. Chloride cycle, *J. Hydrol.*, 207, 56-67, 1998.

615 Hu, Z. L., Islam, S., and Cheng, Y. Z.: Statistical characterization of remotely sensed soil  
616 moisture images, *Remote Sensing of Environment*, 61, 310-318, 1997.

617 Kachanoski, R. G., and Dejong, E.: Scale dependence and the temporal persistence of spatial  
618 patterns of soil-water storage, *Water Resour. Res.*, 24, 85-91, 1988.

619 Kim, G., and Barros, A. P.: Downscaling of remotely sensed soil moisture with a modified  
620 fractal interpolation method using contraction mapping and ancillary data, *Remote Sensing  
621 of Environment*, 83, 400-413, 2002.

622 Koster, R. D., Dirmeyer, P. A., Guo, Z. C., Bonan, G., Chan, E., Cox, P., Gordon, C. T., Kanae,  
623 S., Kowalczyk, E., Lawrence, D., Liu, P., Lu, C. H., Malyshev, S., McAvaney, B., Mitchell,  
624 K., Mocko, D., Oki, T., Oleson, K., Pitman, A., Sud, Y. C., Taylor, C. M., Verseghy, D.,  
625 Vasic, R., Xue, Y. K., Yamada, T., and Team, G.: Regions of strong coupling between soil  
626 moisture and precipitation, *Science*, 305, 1138-1140, 10.1126/science.1100217, 2004.

627 Liu, H. H., and Molz, F. J.: Multifractal analyses of hydraulic conductivity distributions, *Water  
628 Resour. Res.*, 33, 2483-2488, 10.1029/97WR02188, 1997.

629 Mandelbrot, B. B.: *The fractal geometry of nature*, W.H. Freeman and Company, San  
630 Francisco, 1982.

631 Mascaro, G., Vivoni, E. R., and Deidda, R.: Downscaling soil moisture in the southern Great  
632 Plains through a calibrated multifractal model for land surface modeling applications,  
633 *Water Resour. Res.*, 46, W08546, 10.1029/2009WR008855, 2010.

634 Meneveau, C., Sreenivasan, K. R., Kailasnath, P., and Fan, M. S.: Joint multifractal measures:  
635 Theory and applications to turbulence, *Physical Review A*, 41, 894-913, 1990.

636 Montero, E. s.: Rényi dimensions analysis of soil particle-size distributions, *Ecological  
637 Modelling*, 182, 305-315, <http://dx.doi.org/10.1016/j.ecolmodel.2004.04.007>, 2005.

638 National Wetlands Working Group: *The Canadian wetland classification system*, University of  
639 Waterloo, ON, 1997.

640 Pomeroy, J. W., and Gray, D. M.: Snowcover, accumulation, relocation, and management, in:  
641 NHRI Science Report No. 7, Environment Canada, Saskatoon, SK., 144, 1995.

642 Pomeroy, J. W., de Boer, D., and Martz, L. W.: Hydrology and water resources, in:  
643 Saskatchewan: Geographic Perspectives, edited by: Thraves, B., CRRC, Regina, SK,  
644 Canada, 2007.

645 Quinn, P.: Scale appropriate modelling: representing cause-and-effect relationships in nitrate  
646 pollution at the catchment scale for the purpose of catchment scale planning, *J. Hydrol.*,  
647 291, 197-217, 10.1016/j.hydrol.2003.12.040, 2004.

648 Rodriguez-Iturbe, I., Vogel, G. K., Rigon, R., Entekhabi, D., Castelli, F., and Rinaldo, A.: ON  
649 THE SPATIAL-ORGANIZATION OF SOIL-MOISTURE FIELDS, *Geophys. Res. Lett.*,  
650 22, 2757-2760, 10.1029/95gl02779, 1995.

651 Schertzer, D., and Lovejoy, S.: Physical modeling and analysis of rain and clouds by  
652 anisotropic scaling multiplicative processes, *Journal of Geophysical Research:  
653 Atmospheres*, 92, 9693-9714, 10.1029/JD092iD08p09693, 1987.

654 Sivapalan, M.: Scaling of hydrologic parameterizations, 1. Simple models for the scaling of  
655 hydrologic state variables, examples and a case study, Center for Water Research,  
656 University of Western Australia, Nedlands, WA, Australia, 1992.

657 van der Kamp, G., Hayashi, M., and Gallen, D.: Comparing the hydrology of grassed and  
658 cultivated catchments in the semi-arid Canadian prairies, *Hydrol. Proc.*, 17, 559-575,  
659 10.1002/hyp.1157, 2003.  
660 Voss, R.: Fractals in nature: From characterization to simulation, in: *The Science of Fractal*  
661 *Images*, edited by: Peitgen, H.-O., and Saupe, D., Springer New York, 21-70, 1988.  
662 Western, A. W., Grayson, R. B., Bloschl, G., Willgoose, G. R., and McMahon, T. A.: Observed  
663 spatial organization of soil moisture and its relation to terrain indices, *Water Resour. Res.*,  
664 35, 797-810, 1999.  
665 Zeleke, T. B., and Si, B. C.: Scaling properties of topographic indices and crop yield:  
666 Multifractal and joint multifractal approaches, *Agron. J.*, 96, 1082-1090, 2004.

667

## 668 **Figure captions**

669 Fig. 1: Conceptual schematics showing the vegetation growth patterns in the different section  
670 of landscapes at different times of the year. The figure is developed based on field observations  
671 and the scale is arbitrary.

672 Fig. 2. Log-log plot between the aggregated variance of the SWS spatial series and the scale.  
673 A linear relationship indicated the presence of scale invariance and scaling laws for three  
674 selected dates.

675 Fig. 3. Mass exponents for soil water storage spatial series measured at selected 20 cm soil  
676 layer down to 140 cm in 2008 for a range of  $q$  (-15 to 15 at 0.5 increments). The solid line is a  
677 linear reference created following the UM model of Schertzer and Lovejoy (1987) passing  
678 through ( $q = 0$ ).

679 Fig. 4. Mass exponents for selected soil water storage spatial series from surface to different  
680 soil layers (cumulative storage) at 20 cm increment down to 140 cm in 2008 for a range of  $q$  (-  
681 15 to 15 at 0.5 increments). The solid line is a linear reference created following the UM model  
682 of Schertzer and Lovejoy (1987) passing through ( $q = 0$ ).

683 Fig. 5. The width of the multifractal spectrum ( $\alpha_{\max} - \alpha_{\min}$  value) for soil water storage at different depths  
684 (20 cm increment) for all measurements completed during the study period.

685 Fig. 6. Multifractal spectra of soil water storage spatial series measured at each 20 cm soil layer  
686 down to 140 cm in 2008, 2010 and 2011 for a range of  $q$  (-15 to 15 at 0.5 increments).

687 Fig. 7. Multifractal spectra of soil water storage spatial series from surface to different soil  
688 layers (cumulative storage) at 20 cm increment down to 140 cm in 2008, 2010 and 2011 for a  
689 range of  $q$  (-15 to 15 at 0.5 increments).

690 Fig. 8. The information dimension (D1) for soil water storage at different depths (20 cm  
691 increment) over the whole measurement period.

692 Fig. 9. Generalized dimension spectra of soil water storage spatial series measured at each 20  
693 cm soil layer down to 140 cm in 2008 for a range of  $q$  (-15 to 15 at 0.5 increments).

694 Fig. 10. Generalized dimension spectra of soil water storage spatial series from surface to  
695 different soil layers (cumulative storage) at 20 cm increment down to 140 cm in 2008 for a  
696 range of  $q$  (-15 to 15 at 0.5 increments).

697 Fig. 11: Conceptual schematics showing vegetation development over time, dominant water  
698 loss processes and the scaling behavior of soil water storage at different depths. The figure is  
699 developed based on field observations and scaling analysis. The scale of the figure is arbitrary.

## 700 **Tables**

701 Table 1

702 Table 1. Maximum, minimum, and average soil water storage at different depths (20 cm increment) over the whole measurement period.

	0-20 cm			20-40 cm			40-60 cm			60-80 cm			80-100 cm			100-120 cm			120-140 cm		
	Maximum (cm)	Minimum (cm)	Average (cm)	Maximum (cm)	Minimum (cm)	Average (cm)	Maximum (cm)	Minimum (cm)	Average (cm)	Maximum (cm)	Minimum (cm)	Average (cm)	Maximum (cm)	Minimum (cm)	Average (cm)	Maximum (cm)	Minimum (cm)	Average (cm)	Maximum (cm)	Minimum (cm)	Average (cm)
Jul 17 2007	13.96	3.25	5.65	11.55	3.09	5.63	9.43	2.59	5.73	9.06	3.34	5.90	9.51	3.22	5.89	9.81	3.55	6.05	9.81	3.54	6.14
Aug 7 2007	13.96	3.05	4.90	9.28	2.73	5.04	8.30	2.40	5.21	9.36	2.75	5.48	8.23	2.96	5.57	7.52	3.17	5.62	9.11	3.17	5.67
Sept 1 2007	13.96	2.26	5.29	9.28	3.00	5.08	8.08	2.42	5.23	6.98	2.75	5.38	7.17	2.92	5.52	8.08	3.20	5.64	9.07	3.23	5.73
Oct 12 2007	8.30	3.40	5.04	6.92	3.07	5.03	6.74	2.43	5.19	7.60	2.81	5.36	8.39	2.93	5.48	7.92	3.25	5.60	8.55	3.25	5.67
May 2 2008	13.96	4.49	6.28	9.96	4.09	6.03	9.43	3.69	5.80	8.83	3.16	5.74	9.51	2.90	5.66	9.81	3.26	5.70	9.81	3.30	5.75
May 31 2008	13.96	3.30	5.21	9.28	1.54	5.51	8.08	1.58	5.55	6.85	3.00	5.58	7.08	3.08	5.64	8.08	3.22	5.70	8.39	3.25	5.79
Jun 21 2008	8.77	3.06	4.70	7.84	3.43	5.25	6.86	2.80	5.38	6.78	2.77	5.52	7.08	3.04	5.61	7.73	3.28	5.69	8.48	3.23	5.77
July 16 2008	7.07	2.78	4.03	6.78	3.06	4.77	6.71	2.60	5.10	6.75	2.56	5.30	6.84	2.91	5.43	6.98	3.17	5.56	7.01	3.16	5.64
Aug 23 2008	4.96	2.44	3.40	5.66	2.73	4.11	6.02	2.37	4.59	6.44	2.36	4.90	6.56	2.63	5.12	6.85	3.04	5.30	6.81	2.99	5.42
Sept 17 2008	4.64	2.66	3.51	5.63	2.79	4.07	5.91	2.49	4.55	6.28	2.45	4.85	6.59	2.63	5.05	6.68	3.05	5.25	6.91	2.96	5.37
Oct 22 2008	6.11	3.83	4.96	6.03	3.10	4.37	5.92	2.52	4.53	6.13	2.46	4.79	6.55	2.63	5.00	6.61	3.00	5.18	6.73	1.22	5.28
April 20 2009	13.96	4.73	6.67	11.55	3.62	5.84	10.49	3.23	5.62	8.83	2.97	5.48	9.51	2.67	5.38	9.81	3.08	5.49	9.81	2.85	5.66
May 7 2009	13.96	4.45	5.97	9.51	3.68	5.70	8.08	3.26	5.49	8.30	3.00	5.36	7.85	2.73	5.35	9.81	3.01	5.43	8.91	2.84	5.51
May 27 2009	12.60	3.67	5.43	8.15	3.55	5.52	8.08	3.43	5.39	6.78	3.13	5.37	7.16	2.64	5.39	8.08	2.96	5.51	8.45	2.80	5.53
July 21 2009	6.92	3.16	4.56	7.24	3.16	4.83	6.55	2.91	5.00	6.72	2.95	5.23	6.77	2.58	5.24	6.91	3.02	5.34	6.89	3.24	5.43
Aug 27 2009	6.64	3.42	5.01	6.67	3.57	5.07	6.32	2.84	4.92	6.50	2.85	5.03	6.76	2.57	5.16	6.79	3.00	5.25	6.90	3.02	5.34
Oct 27 2009	6.65	3.89	5.30	6.44	3.44	4.90	6.04	2.74	4.80	6.36	2.68	4.91	6.55	2.60	5.05	6.71	3.05	5.17	6.71	2.79	5.29
April 6 2010	13.96	4.67	6.47	9.51	3.53	5.52	9.43	3.19	5.31	8.83	2.91	5.35	9.51	2.61	5.23	9.81	3.01	5.34	9.81	2.83	5.41
May 19 2010	13.96	4.08	6.04	11.32	4.28	5.94	10.49	4.46	5.94	8.75	4.08	5.93	8.60	3.55	5.90	9.81	4.03	5.91	9.81	3.96	5.85
June 14 2010	13.96	4.38	6.54	11.55	4.48	6.32	10.49	4.58	6.31	8.83	4.27	6.29	9.51	3.86	6.22	9.81	4.37	6.24	9.81	4.50	6.20
Sept 28, 2010	13.96	4.51	6.33	11.55	4.48	6.16	9.43	3.77	6.08	8.83	3.91	6.13	9.51	3.83	6.12	9.81	4.11	6.16	9.79	4.18	6.20
May 13, 2011	13.96	4.82	7.12	11.55	4.87	6.61	10.49	4.75	6.50	9.21	4.54	6.40	9.51	4.16	6.34	9.96	3.17	6.32	9.79	4.30	6.45
Jun 6, 2011	13.96	4.31	7.05	11.55	4.56	6.59	10.49	3.85	6.52	9.06	4.75	6.44	9.51	4.21	6.40	9.96	3.17	6.39	9.79	4.77	6.52
Jun 29, 2011	13.96	4.93	7.16	11.55	4.96	6.73	10.49	4.29	6.64	9.74	4.42	6.57	9.51	4.28	6.49	9.96	3.17	6.46	9.79	4.30	6.55
Sept 29, 2011	12.60	3.11	5.25	8.15	3.46	5.50	8.08	2.88	5.68	7.58	4.03	5.82	9.19	3.77	5.89	9.51	3.81	6.02	9.36	4.14	6.04
5 year average			5.51			5.45			5.48			5.56			5.61			5.69			5.77

704 Table 2: Correlation coefficients between joint multifractal indices ( $\alpha$  and  $\beta$ ) of the surface  
 705 layer with those from subsurface layers at 20cm intervals in 2008. The number of data points  
 706 are same for all the analysis.

	2 May 2008	31 May 2008	21 Jun. 2008	16 Jul. 2008	23 Aug. 2008	17 Sep. 2008	22 Oct. 2008
0-20 cm vs. 20-40 cm	0.96	0.98	0.99	0.99	0.99	1.00	1.00
0-20 cm vs. 40-60 cm	0.93	0.96	0.96	0.97	0.97	1.00	1.00
0-20 cm vs. 60-80 cm	0.93	0.94	0.95	0.95	0.96	0.99	0.99
0-20 cm vs. 80-100 cm	0.92	0.92	0.93	0.94	0.94	0.98	0.99
0-20 cm vs. 100-120 cm	0.92	0.92	0.93	0.93	0.93	0.97	0.99
0-20 cm vs. 120-140 cm	0.93	0.94	0.95	0.94	0.94	1.00	1.00

707

708

709

710

711

712

713

714

715

716

717

718

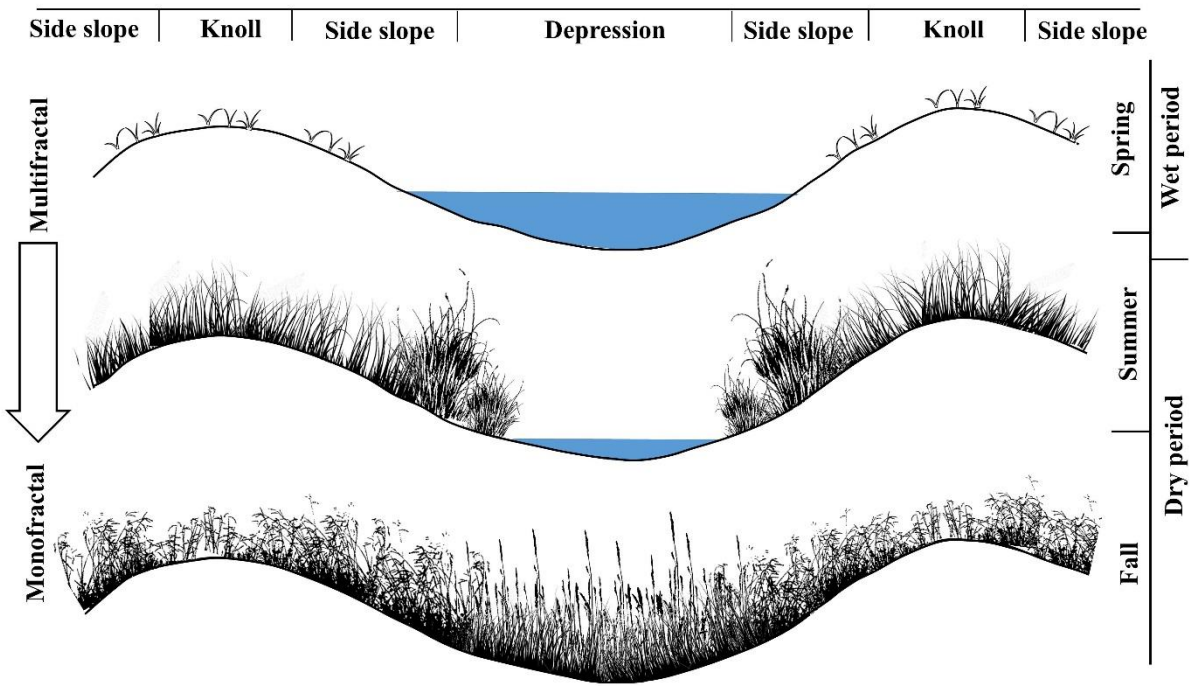
719

720



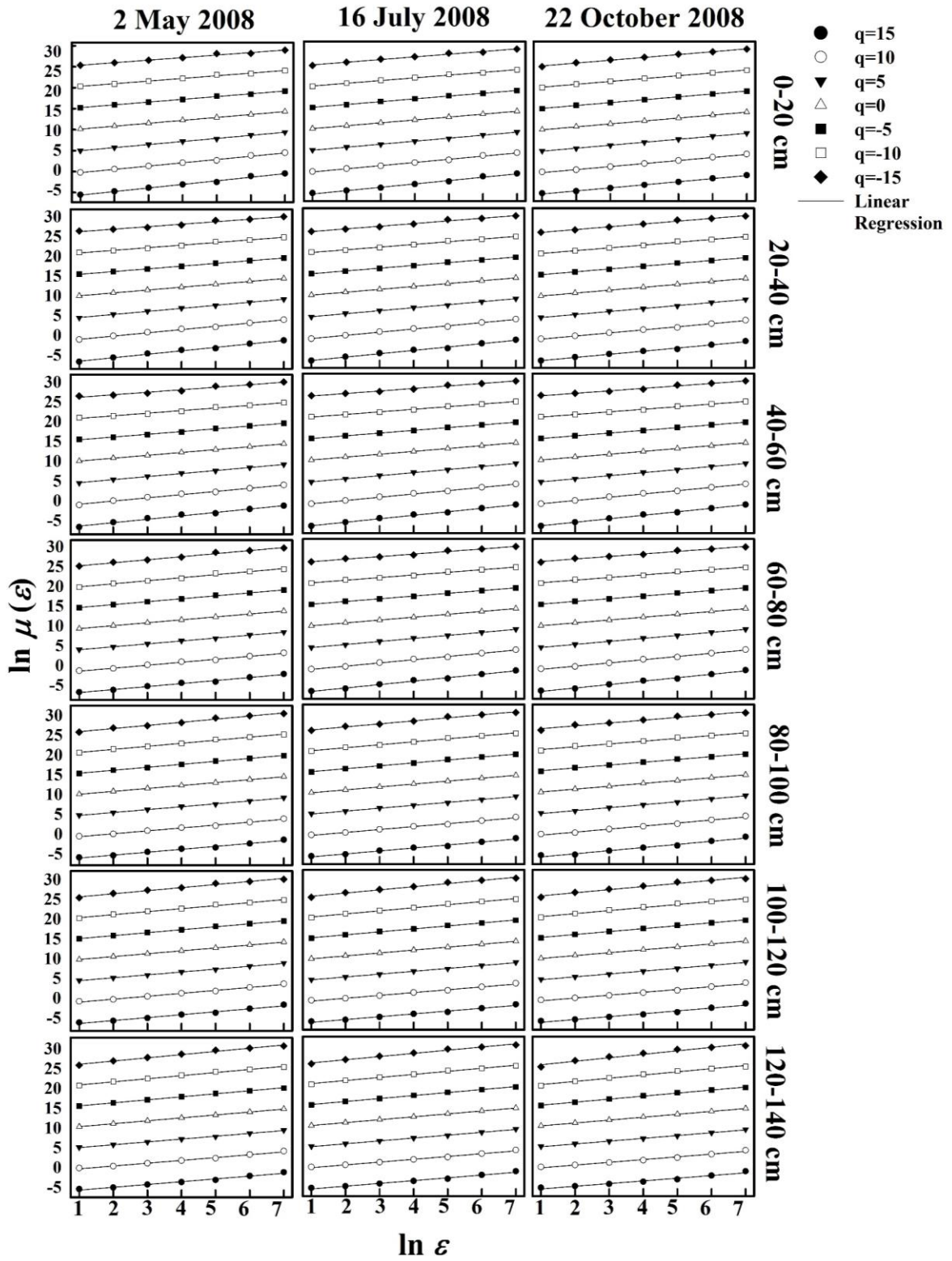
721

722 **Figures**



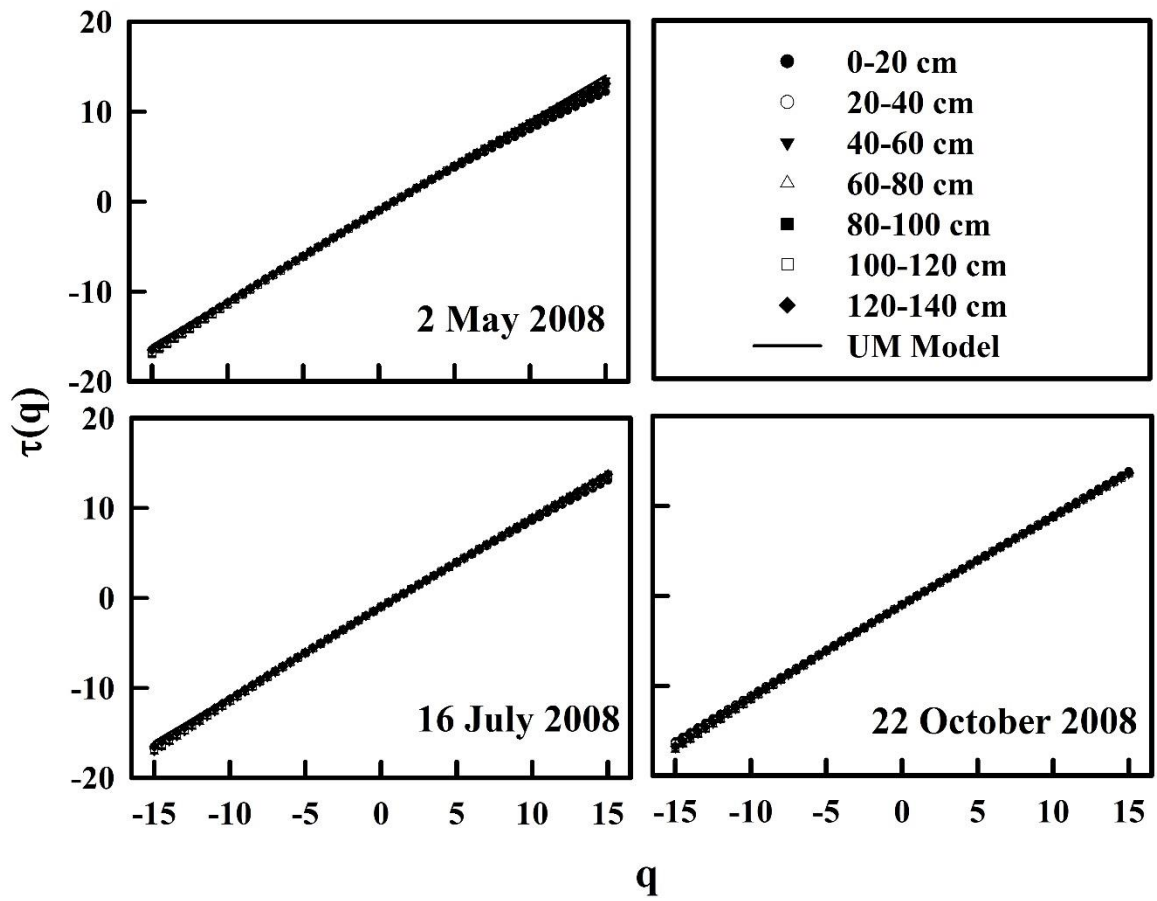
723

724 **Figure 1**



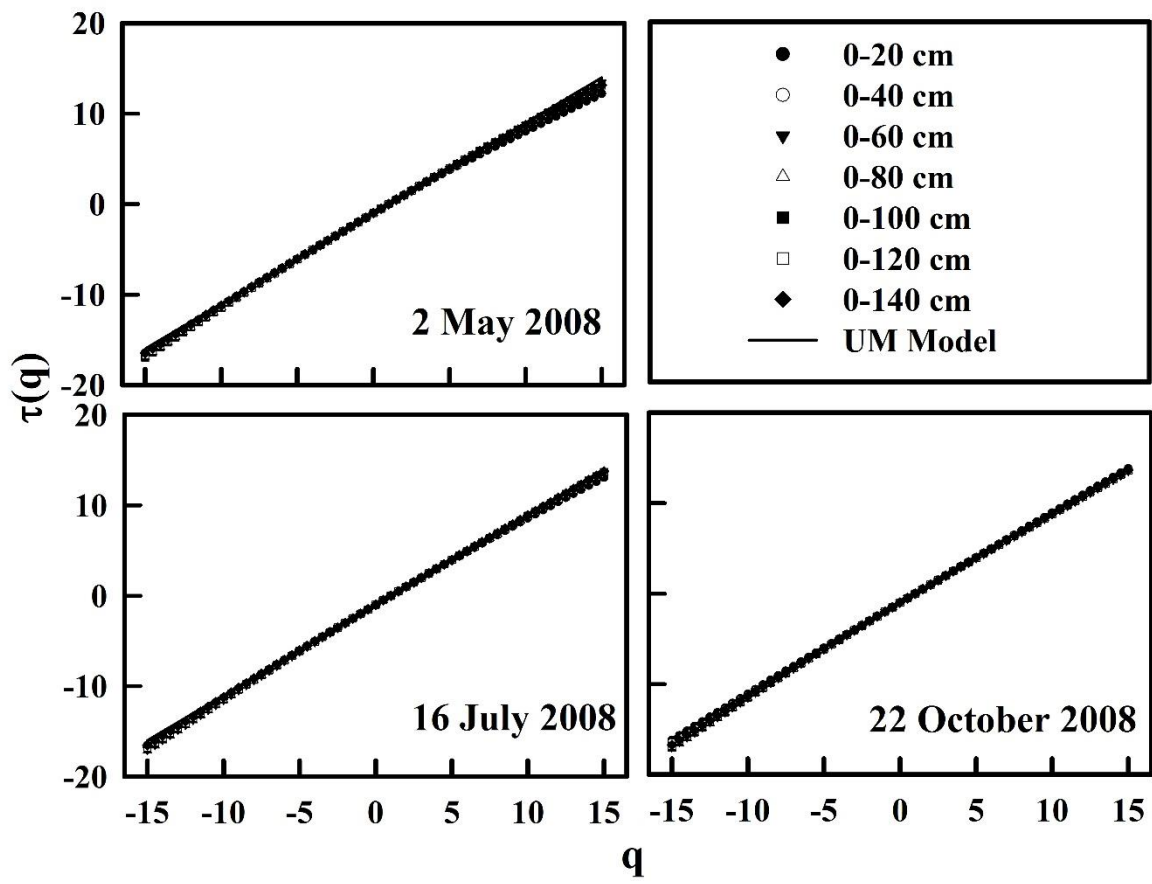
725

726 Figure 2



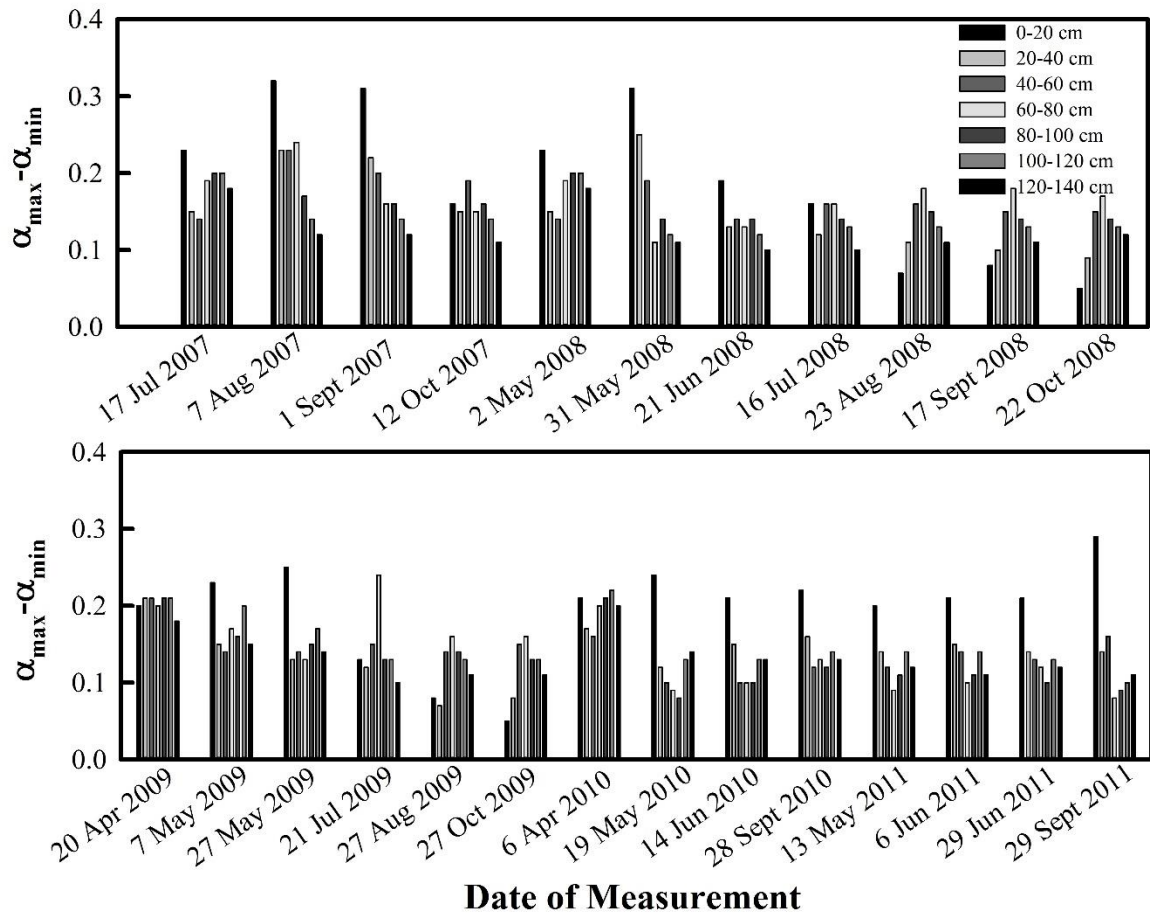
727

728 Figure 3



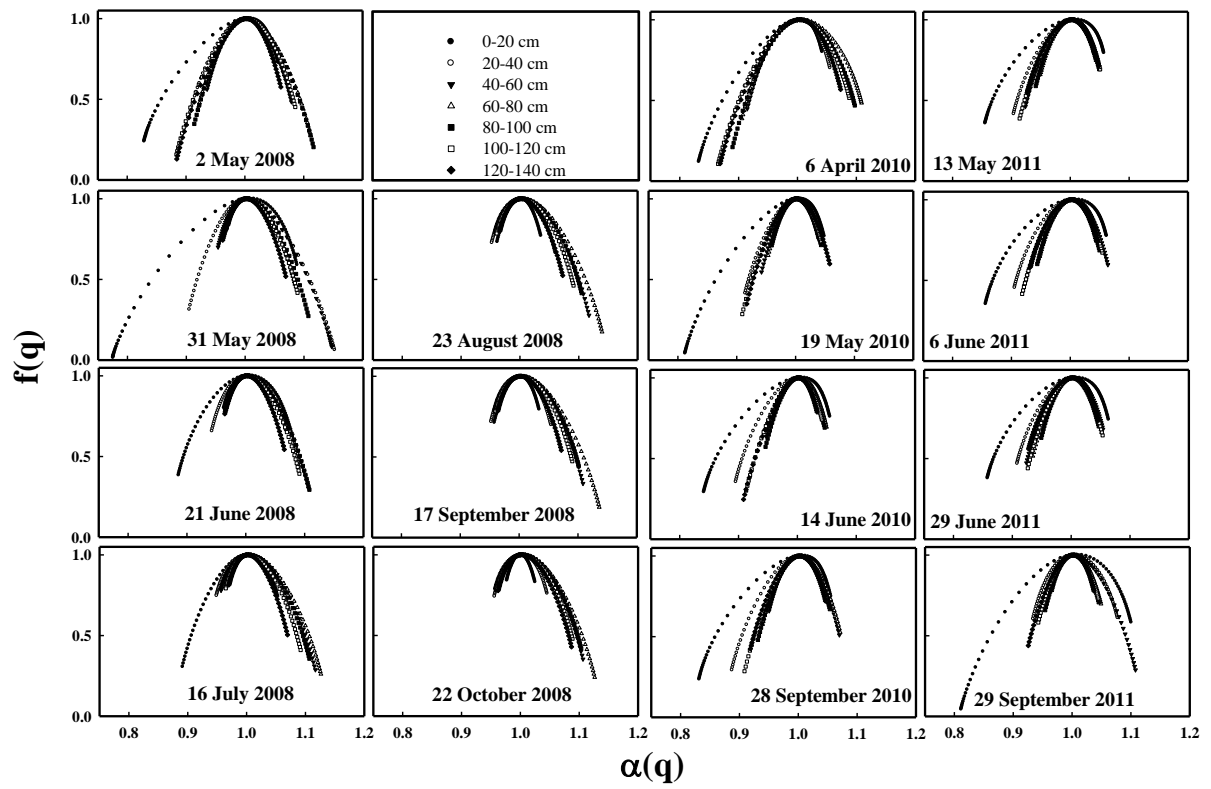
729

730 Figure 4



731

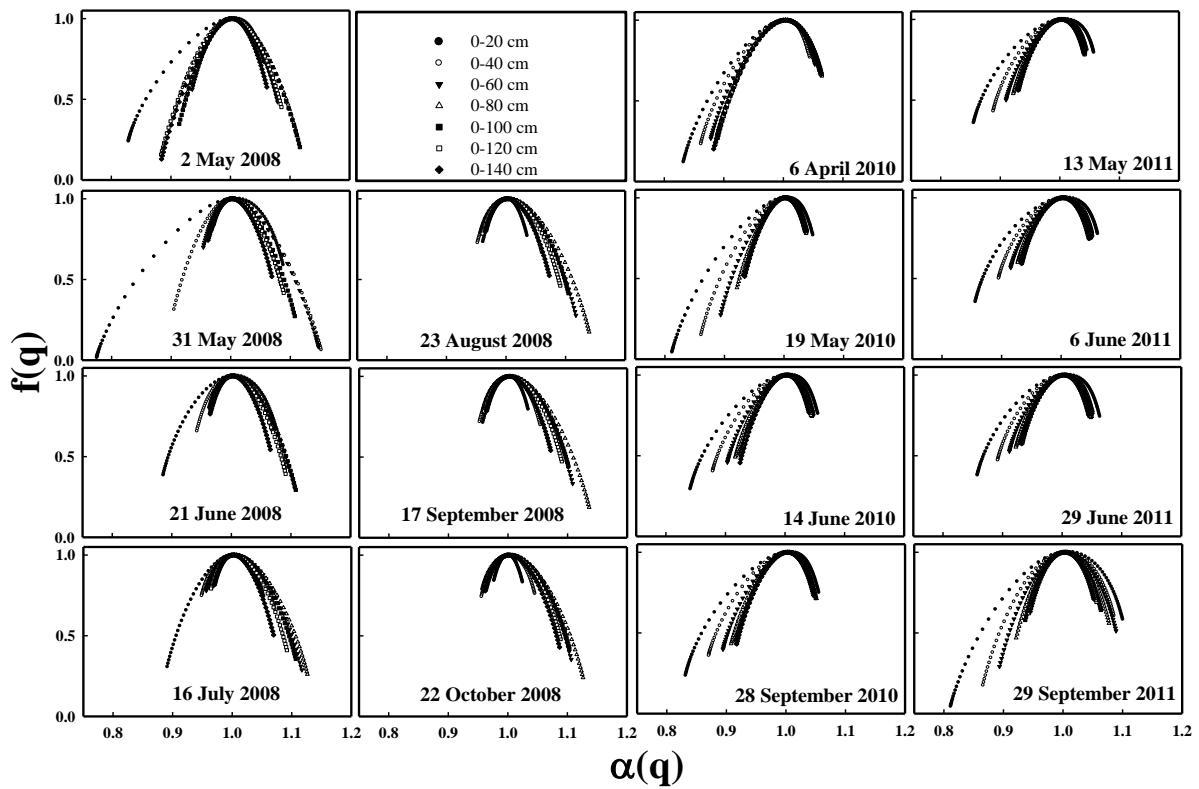
732 Figure 5



733

734

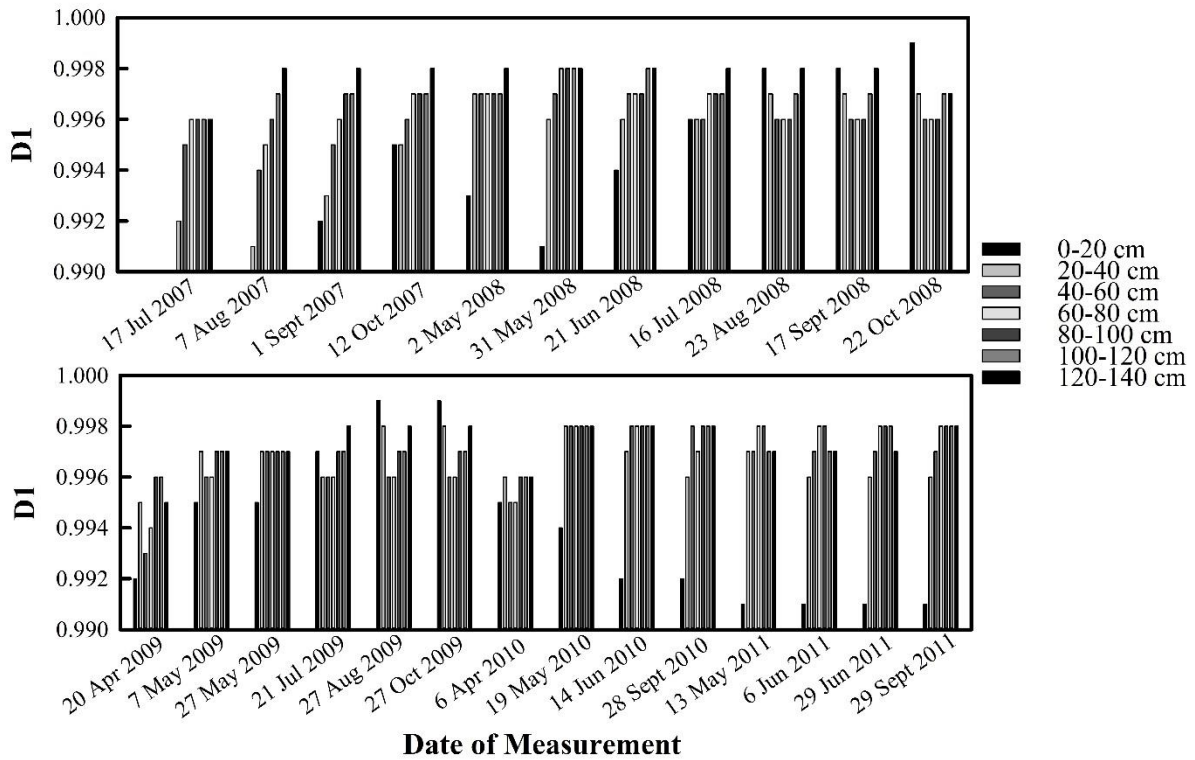
735 Figure 6



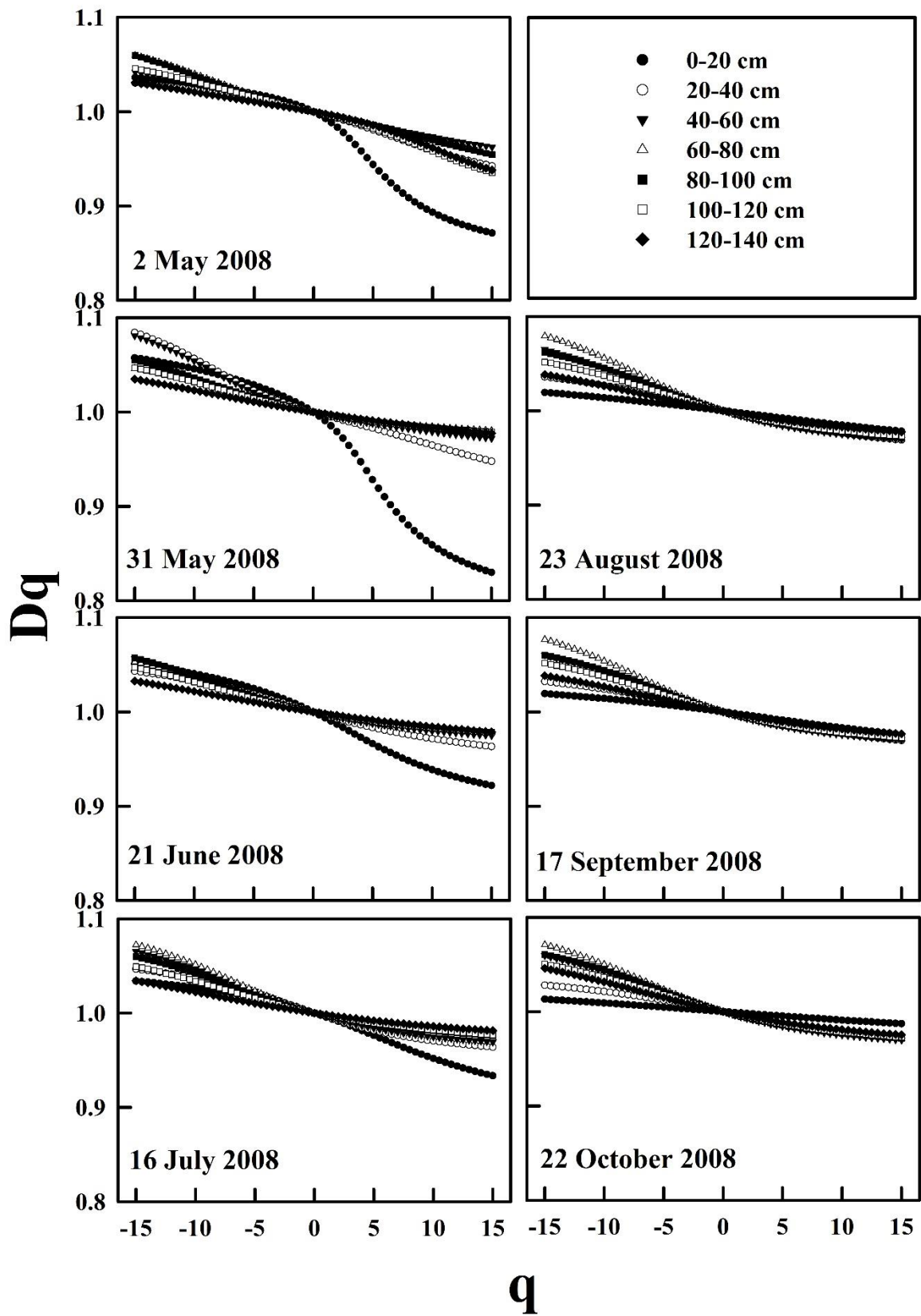
736

737

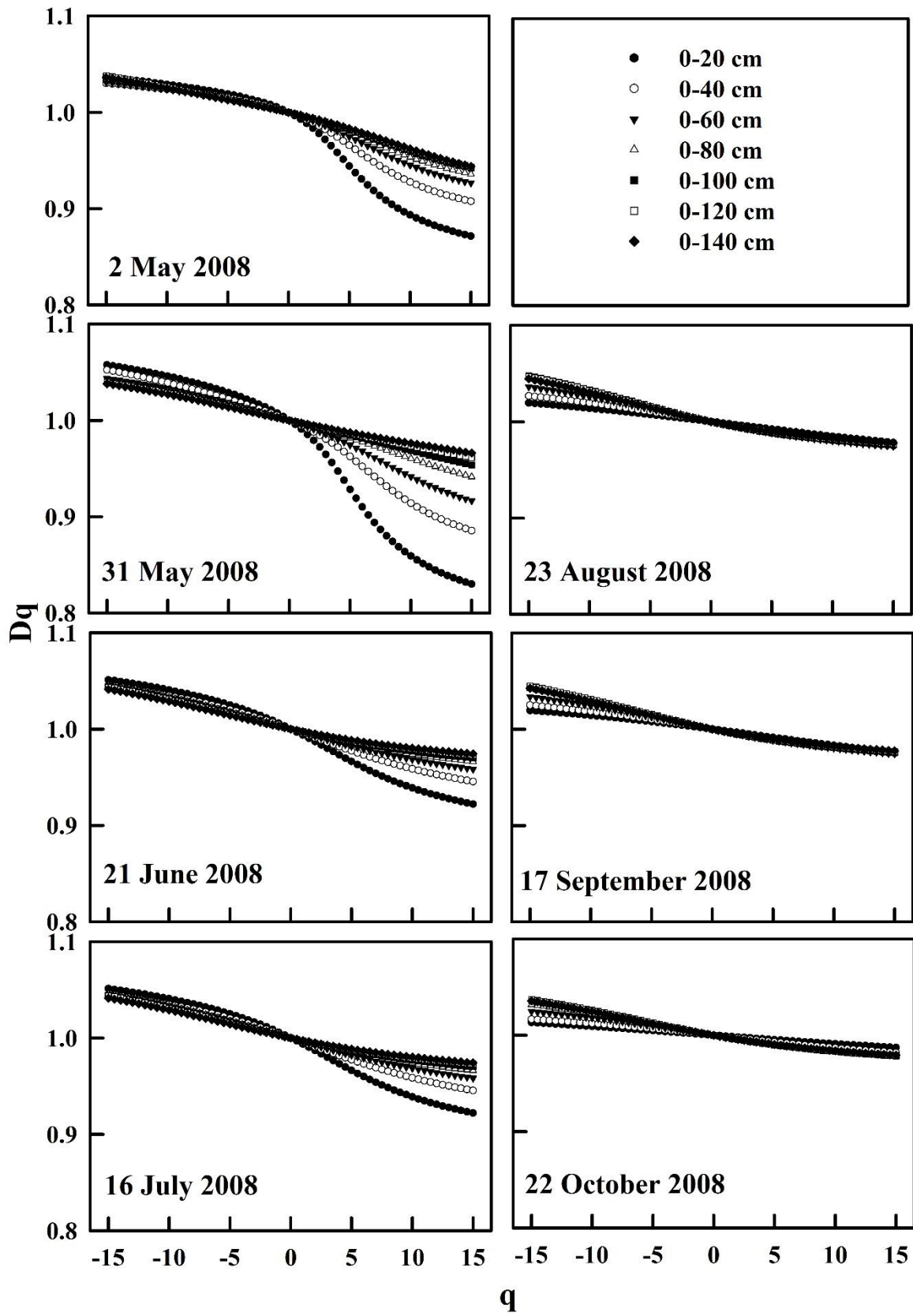
738 Figure 7

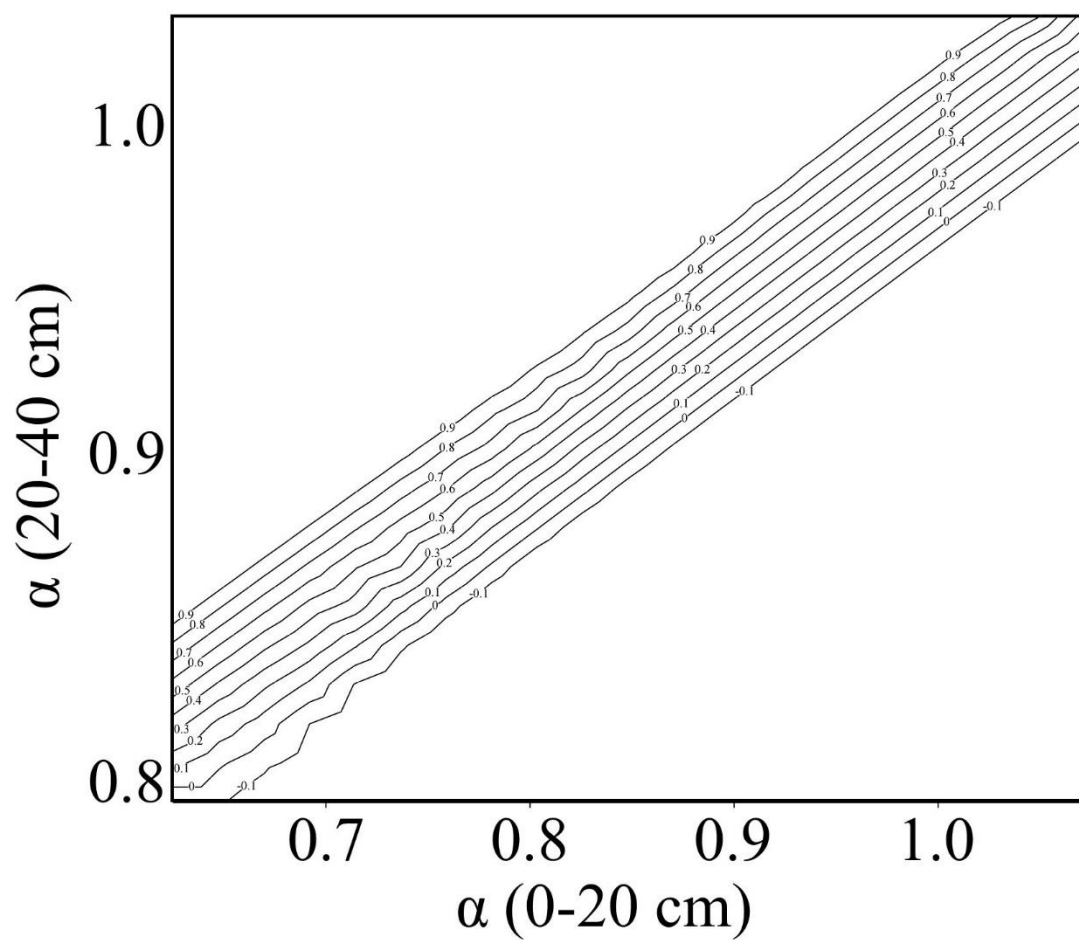


739



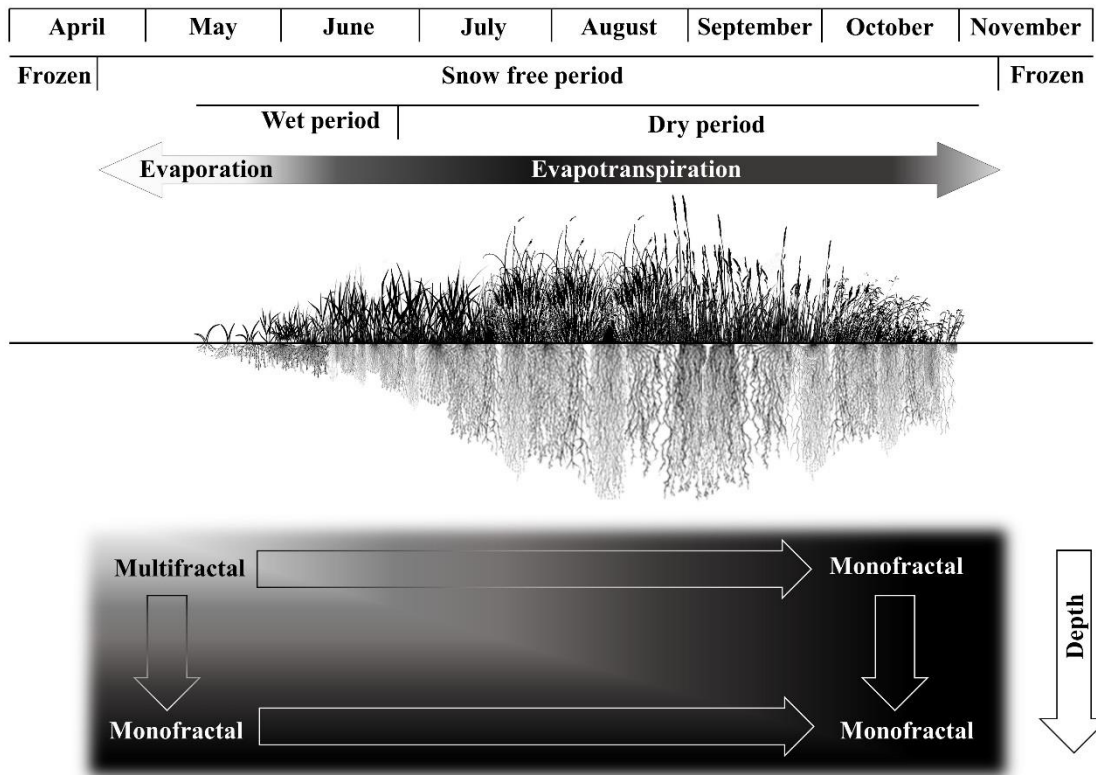






746

748



749

750 Figure 12